

Article

# Predictive Extended State Observer-Based Active Disturbance Rejection Control for Systems with Time Delay

Syeda Nadiah Fatima Nahri , Shengzhi Du \* and Barend J. van WykDepartment of Electrical Engineering, Faculty of Engineering and the Built Environment,  
Tshwane University of Technology, Pretoria 0183, South Africa

\* Correspondence: dus@tut.ac.za

**Abstract:** The latest research on disturbance rejection mechanisms has shown active disturbance rejection control (ADRC) to be an effective controller for uncertainties and nonlinear dynamics embedded in systems to be controlled. The significance of the ADRC controller is its model-free nature, as it requires minimal knowledge of the system model. In addition, it can actively estimate and compensate for the impact of internal and external disturbances present, with the aid of its crucial subsystem called the extended state observer (ESO). However, ADRC controller design becomes more challenging owing to different system disturbances, such as output disturbances, measurement noise, and varying time-delays persistent in the system's communication channels. Most disturbance rejection techniques aim to reduce internal perturbations and external disturbances (input and output disturbance). However, output disturbance rejection with measurement noise under time-delay control is still a challenging problem. This paper presents a novel predictive ESO-based ADRC controller for time-delay systems by employing predictive methods to compensate for the disturbances originating from time delay. The prediction mechanism of the novel (proposed) controller design is greatly attributed to the extended state predictor observer (ESPO) integrated with the delay-based ADRC inside the proposed controller method. Thus, the proposed controller can predict the unknown system dynamics generated during the delay and compensate for these dynamics via disturbance rejection under time-delay control. This approach uses the optimization mechanism to determine controller parameters, where the genetic algorithm (GA) is employed with the integral of time-weighted absolute error (ITAE) as the fitness function. The proposed controller is validated by controlling second-order systems with time delay. Type 0, Type 1, and Type 2 systems are considered as the controlled plants, with disturbances (unknown dynamics due to delay and external disturbance), along with measurement noise present. The proposed controller method is compared with state-of-the-art methods, such as the modified time-delay-based ADRC method and the ESPO-based controller method. The findings indicate that the method proposed in this paper outperforms its existing competitors by compensating for the dynamics during the time delay and shows robust behaviour, improved disturbance rejection, and a fair extent of resilience to noise.

**Keywords:** modified time-delay-based ADRC; time-delay control; predictive ESO-based ADRC; extended state predictor observer (ESPO); disturbance compensation; measurement noise



**Citation:** Nahri, S.N.F.; Du, S.; van Wyk, B.J. Predictive Extended State Observer-Based Active Disturbance Rejection Control for Systems with Time Delay. *Machines* **2023**, *11*, 144. <https://doi.org/10.3390/machines11020144>

Academic Editor: Zheng Chen

Received: 28 November 2022

Revised: 13 January 2023

Accepted: 17 January 2023

Published: 20 January 2023



**Copyright:** © 2023 by the authors. Licensee MDPI, Basel, Switzerland. This article is an open access article distributed under the terms and conditions of the Creative Commons Attribution (CC BY) license (<https://creativecommons.org/licenses/by/4.0/>).

## 1. Introduction

In the field of robotics, automation, and teleoperation systems, the presence of time delay is greatly attributed to the inefficient operation of a system [1–3]. Therefore, various model-based and model-free control methods have been developed over time. A system's parameter uncertainties and unmodelled dynamics affect the former control method. In contrast, the latter method considers various system uncertainties, such as internal perturbations, external disturbances, unmodelled dynamics, and nonlinearity [4]. One widely developed model-free controller is active disturbance rejection control (ADRC), whose model has been modified over time to execute time-delay and disturbance compensations.

The ADRC controller was first discovered and introduced by Han in 1995 [5,6], followed by complete implementations by Gao in 2009 [7,8], wherein the ADRC is shown independent of the model parameters of the controlled system. The ADRC contains an important feature called the extended state observer (ESO), which can estimate the system states and disturbances in real time, followed by the total disturbance compensation via the feedback loop [6]. In this way, ADRC rejects different forms of disturbances, such as parameter perturbations, unknown system dynamics, and internal or external disturbances for both linear and nonlinear systems [7,9]. Over time, the ADRC controller having an  $n$ -order design has been used for  $n$ -state systems (for  $n \geq 1$ ) [10–12]. The importance of ADRC design has been highlighted in scenarios involving practical applications and areas of academic research [13–17]. Several industrial applications, such as nuclear reactors, thermal power plants, medical practice, speed control processes, uncertain robotic systems, and teleoperation applications, were successfully controlled by the ADRC.

The presence of time delay and its impacts on real-world systems are inevitable. For example, time delay negatively affects the control performance in various aspects, such as reduced damping ratio for a closed-loop system showing a more oscillatory response, increased percentage overshoot, and shifting the system closer to instability in the closed-loop response [18]. In addition, the presence of these perturbations, as mentioned earlier, often complicates the control system design. Thus, proposing a controller that provides a decent control performance in the vicinity of time-delay effects and other uncertainties has been a major global attraction for scholars. With this in mind, ADRC time-delay control has evolved and developed recently to minimize the detrimental effects of time delay and time-varying time-delay scenarios while keeping the disturbance compensation mechanism [7,19–21].

### 1.1. Related ADRC Works

This subsection briefly explains ADRC-related works on time-delay compensation and disturbance compensation mechanisms by both non-predictive and predictive-based methods found in recent literature.

Different predictors were computed using both the input and output of the controlled object, and their output was fed to the ESO of the ADRC to form a predictive ADRC. Here the predictive ESO of the ADRC is designed by treating the disturbances and parametric uncertainties associated with the processes as an extended state variable to be estimated in real time using ESO. In [22], delay-less estimation of total disturbance is attained, maintaining its stability margin and a better response than normal ESO. In [23], the combination of a new Smith predictor (SP) with linear ADRC is proposed to improve the time synchronization between the two input signals of the linear ESO. In [24], a predictor is designed to obtain system state estimation and mismatched disturbance estimation values. In addition, the output predictor is used to compensate for the influences of measurement delay and sampling of output. In addition, more predictive ESO designs include consensus protocols with delays and disturbances, designs based on the repetitive controller for rejection of periodic signals under long input delays, and discrete control to prove the MIMO system's stability, as seen in [25–27].

Further, other predictive ADRC methods evolved include the Smith predictor-based ADRC (SP-ADRC) [28], predictor observer/extended state predictor observer-based ADRC (PO/ESPO ADRC) [29], polynomial-based predictive ADRC (PP-ADRC) [30], predictive-generalized ADRC [31,32], and internal model control (IMC) interpretation of several linear ADRCs [33], to name a few. These methods proposed various strategies to deal with time delay and uncertainties. In [28], a Smith predictor (SP) was introduced before the ESO. However, this is heavily dependent on a nominal stable plant model, resulting in oscillations due to model mismatch, which restricts the target tracking error convergence rate of SP-ADRC [34]. On the other hand, PO-ADRC achieves fast convergence of tracking error and stability, independent of time delay. Even though this method effectively rejects uncertain dynamics and noise associated with sensor delay, further theoretical analysis

is required to determine its optimal parameters [20,29]. Additionally, IMC configuration was used to tune the modified PP-ADRC [33], where the time-delay term is approximated by a polynomial using Taylor expansion seen in [7] or Pade approximation seen in [30]. Despite being straightforward, the IMC-related PP-ADRC structure needs improvement in disturbance rejection and tracking performance. It was shown that PO-ADRC has a better delay compensation mechanism than the SP-ADRC and DD-ADRC structures. However, its parameters must be carefully tuned to achieve an acceptable performance.

Furthermore, some popular non-predictive ADRC time-delay-related works include delay-designed ADRC (DD-ADRC) and its IMC structure [33,35]. To obtain synchronous ESO input signals for DD-ADRC, the control signal was delayed to match the time delay in the plant [35]. This strengthens stability and time-delay compensation, but the performance depends on how big the time-delay and output disturbance intensity is [20]. Some other methods include sliding mode control-based ADRC [36], ADRC for uncertain nonlinear time-delay systems where the upper bound of ESO gains depends on small input delay values [37], and ADRC with modified twice optimal control (ADRC-MTOC) [38]. The ADRC-MTOC design showed strong disturbance rejection capacity and fast recovery time [38]. However, future work demands performance improvement in the initial stages of response and stable output disturbance rejection.

### *1.2. Novelty and Contribution of This Paper*

In addition to the time delay, disturbances in the form of uncertainties and unknown dynamics have a significant impact on the controller design. To achieve stability and effective controller operation, time-delay compensation and disturbance compensation are thus tightly related. Some of the related ADRC works have certain drawbacks. To begin with, several ADRC time-delay-based techniques that delayed the control signal neglected the dynamics that occurred during the delay. In addition, much of the existing research primarily considers the input delay. However, the presence of output system delay with measurement noise is receiving more attention. Further, while there is a physical difference between time-delay (lag) and prediction (lead), the latter is difficult to achieve. Prediction requires more room for improvement than delay because it is more challenging to implement. Most disturbance rejection methods intend to suppress both internal (initial states and parameter perturbations) and external disturbances (input and output disturbance). However, output disturbance rejection under time-delay control is still a challenging issue.

As a result, the objective of the paper is to construct a novel predictive-based ADRC controller design constituting a model-free time-delay-based ADRC approach cascaded with a model-based ESPO (extended state predictor observer) method. The novelty of this proposed controller design (called the predictive ESO-based ADRC controller) is attributed to its predictive feature; that is, it predicts the unknown system dynamics generated during the delay and compensates them as a disturbance under time-delay control. Firstly, this disturbance compensation is achieved by feeding the unknown system dynamics (due to the delay) to the ESPO inside the novel integrated (proposed) controller design. Secondly, the predicted plant output generated by the ESPO is fed to the novel ESO of the proposed controller. Lastly, the total predicted disturbance (inclusive of all uncertainties, such as unknown dynamics due to delay, external disturbance, and noise) obtained from one of the two ESPO outputs is subtracted from the ADRC control signal to help with the complete disturbance compensation under time-delay control. To the best of the authors' knowledge, the proposed design that follows the predictive idea for both time-delay and disturbance compensation has not been discussed in previous ADRC works. Therefore, the performance of the proposed methodology is compared with the ESPO and the modified time-delay-based ADRC methods. The experiments conducted for this work are categorized as separate case studies that address the various Type 0, Type 1, and Type 2 second-order control systems. Experiment results show that the proposed controller method improves the stability of transient response, efficiently compensates

for disturbances and measurement noise, shows adequate robustness, and attains quick recovery from disturbance effect under time delay.

The remainder of the paper is structured as follows: Section 2 presents the preliminary concepts used to build the proposed controller design. Section 3 explains the novel (proposed) controller design and algorithm obtained by hybridizing delay-based ADRC and ESPO methods. Results of the comparative study for different types of second-order systems are highlighted in Section 4. The results verifying the validity of the proposed controller configuration are discussed in Section 5. Finally, the conclusion and future works are put forth in Section 6.

## 2. Preliminary Concepts Used in the Proposed Controller Design

This section describes two different controller algorithms and some predominant mathematical concepts used together to build the proposed controller design introduced in Section 3 of this article.

### 2.1. Conventional ADRC

A typical ADRC executes the disturbance rejection mechanism using its model-free method that requires little to no prior knowledge of the object to be controlled. An ADRC controller’s order often corresponds to the relative order of the plant or system to be controlled. Any system with an order greater than two can be analyzed using its second-order approximation [39]. Figure 1 presents a standard second-order ADRC structure composed of the tracking differentiator (TD), the ESO, and the nonlinear state error feedback (NLSEF) controller. The controlled object seen here is a second-order system or a second-order approximation of a higher-order system.

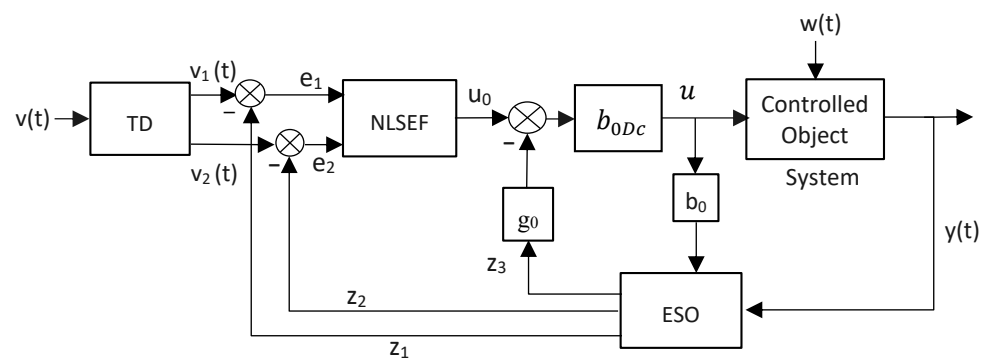


Figure 1. Conventional second-order ADRC structure for a given system.

The model of the system or object to be controlled (seen in Figure 1) is a second-order single-input–single-output (SISO) system and is represented by Equation (1) [40]:

$$\begin{cases} \dot{x}_1 = x_2 \\ \dot{x}_2 = f(x_1, x_2, w(t), t) + bu \\ y = x_1 \end{cases} \quad (1)$$

where  $x$ ,  $y$ ,  $w(t)$ ,  $b$ , and  $u$  are the systems states, output variable, external disturbance, magnification factor, and control variable, respectively. The total internal and external disturbances function is denoted by  $f(x_1, x_2, w(t), t)$ . The structural components and their algorithms of a conventional second-order ADRC design seen in Figure 1 are as follows:

(1) Tracking differentiator (TD): When the reference signal given by  $v(t)$  passes through the TD, it is softened to signal  $v_1(t)$ , and a differentiated signal  $v_2(t)$  is obtained, as seen in Figure 1. In this way, the TD provides a desired transient profile and an improved response of the reference input signal [7]. Equations (2) and (3) provide the desired transient profile

that the output of the plant (controlled object) can adequately follow. Continuous-time representation of the TD is given by Equation (2):

$$\begin{cases} \dot{v}_1 = v_2 \\ \dot{v}_2 = -r \operatorname{sign}\left(v_1 - v(t) + \frac{v_2|v_2|}{2r}\right) \end{cases} \quad (2)$$

where  $v(t)$  is the control objective,  $v_1$  is the desired trajectory, and  $v_2$  is its derivative. Parameter  $r$  is chosen to accelerate or decelerate the transient profile. However, time-optimal solution in continuous time ( $\dot{v}_2$ ) can cause significant numerical inaccuracies in a discrete-time implementation. This discrete-time implementation is given by Equation (3):

$$\begin{cases} v_1(k+1) = v_1(k) + h \cdot v_2 \\ v_2(k+1) = v_2(k) + h \cdot \operatorname{fhan}(v_1(k) - v(k), v_2(k), r_0, h) \end{cases} \quad (3)$$

Hence, to address the numerical error in discrete time, the term  $\operatorname{fhan}(v_1(k) - v(k), v_2(k), r_0, h)$  is provided in Equation (3), where the two important TD controller parameters are  $r_0$  and  $h$ , which provide the speed of the transition process and the simulation step, respectively. For the sake of simplicity, the discrete time is ignored, so  $v$ ,  $v_1$ , and  $v_2$  instead of  $v(k)$ ,  $v_1(k)$ , and  $v_2(k)$  are used in the rest of the paper. The remaining variables  $r_0$  and  $h$  are treated as they are.

By setting  $r_0$  to  $r$  and for a given  $h$ , the fastest convergence from  $v_1$  to  $v$  with no overshoot is obtained by the nonlinear function, “ $\operatorname{fhan}(v_1 - v, v_2, r_0, h)$ ” in Equation (4). This time-optimal solution is calculated step-by-step using the set of relations in Equation (4) [41]:

$$\begin{cases} d = r_0 h^2 \\ a_0 = h v_2 \\ y = v_1 - v + a_0 \\ a_1 = \sqrt{d(d + 8|y|)} \\ a_2 = a_0 + \left[ \frac{\operatorname{sign}(y)(a_1 - d)}{2} \right] \\ s_y = \frac{[\operatorname{sign}(y+d) - \operatorname{sign}(y-d)]}{2} \\ a = (a_0 + y - a_2) s_y + a_2 \\ s_a = \frac{[\operatorname{sign}(a+d) - \operatorname{sign}(a-d)]}{2} \\ \operatorname{fhan} = -r_0 \left( \frac{a}{d} - \operatorname{sign}(a) \right) s_a - r_0 \operatorname{sign}(a) \end{cases} \quad (4)$$

(2) Nonlinear state error feedback (NLSEF) controller: The NLSEF controller improves the proportional–integral–derivative (PID) controller’s control law which has long been a standard in the industry, mainly because of its ability to handle state errors in the past, present, and future times. However, the PID fails to update its parameters in real time to achieve the required performance. Therefore, the nonlinear functions are proposed in Equation (5) [7]:

$$\begin{cases} \operatorname{fal}(e, \alpha, \varepsilon) = \begin{cases} \frac{e}{d^{1-\alpha}}, & |e| \leq \varepsilon \\ |e|^\alpha \operatorname{sign}(e), & |e| > \varepsilon \end{cases} \\ \operatorname{fhan}(v_1 - v, v_2, r, h_1) \end{cases} \quad (5)$$

where  $\alpha$  is the tuning parameter and  $e$  is the error and must attain zero quickly for  $\alpha < 1$ .  $r$  is the control gain, and  $h_1$  is the precision factor. The “ $\operatorname{fhan}$ ” function is computed the same way as Equation (4), containing the NLSEF parameters  $r$  and  $h_1$ .

The NLSEF receives the difference between the signals generated from the TD and the estimated system states ( $z_1$  and  $z_2$  in Figure 1) obtained from the ESO, to generate the control variable ( $u_o$  in Figure 1). Thus, inputs to the NLSEF controller are the difference signals  $e_1$  and  $e_2$  as seen in Figure 1. The disturbance  $w(t)$  is then compensated by the

estimated total disturbance ( $z_3$  in Figure 1) from the control variable ( $u_o$ ) in real time. Thus, the NLSEF is given by the following equations in Equation (6):

$$\begin{cases} e_1 = v_1 - z_1 \\ e_2 = v_2 - z_2 \\ u_o = -\text{fhan}(e_1, c \cdot e_2, r, h_1) \end{cases} \quad (6)$$

where  $c$  is the damping coefficient and  $u_o$  is the control volume or the output of the NLSEF controller.

Controller parameters  $c$ ,  $r$ , and  $h_1$  can be varied from system to system. Therefore, the actual control variable “ $u$ ” is generated and applied to the controlled object, as seen in Figure 1. Because the nonlinear controller (NLSEF) can achieve zero steady-state error (SSE) in a finite amount of time, it is employed instead of a linear controller (LSEF), which is why the NLSEF outperforms the PID controller.

(3) Extended state observer (ESO): The ESO is a crucial subsystem of the ADRC, with minimum dependence on the system details. It estimates the system state variables ( $z_1$  and  $z_2$  in Figure 1) and observes the total disturbance ( $z_3$  in Figure 1) in real time, as shown in Equation (7) [42]. The total disturbance includes uncertainties such as unmodelled dynamics, internal disturbances (internal perturbations), and external disturbances.

$$\begin{cases} e = z_1 - y \\ \dot{z}_1 = z_2 - \beta_{01}e \\ \dot{z}_2 = z_3 - \beta_{02}fe + b_0u \\ \dot{z}_3 = -\beta_{03}fe_1 \end{cases} \quad (7)$$

where  $\beta_{01}$ ,  $\beta_{02}$  and  $\beta_{03}$  are ESO design parameters (also called observer gains) and are related to the ESO bandwidth [7]. These ESO parameters have no fixed values and can be selected differently as per a specific problem. In [7], various relations in terms of ESO simulation step size ( $h_{\text{ESO}}$ ) have been provided to obtain  $\beta_{01}$ ,  $\beta_{02}$ , and  $\beta_{03}$ .  $u$  is the input,  $y$  is the controlled object output, and  $b_0$  is the gain factor, as seen in Figure 1. Nonlinear feedback functions “ $fe$ ” and “ $fe_1$ ” are indicated by Equation (8):

$$\begin{cases} fe = \text{fal}(e, 0.5, h_{\text{ESO}}) \\ fe_1 = \text{fal}(e, 0.25, h_{\text{ESO}}) \end{cases} \quad (8)$$

From Figure 1, one obtains the control law of the ADRC seen in Equation (9):

$$u = (u_o - z_3g_0)b_{0Dc} \quad (9)$$

where  $g_0$  and  $b_{0Dc}$  are the gain factor and disturbance compensation factor of the ADRC, respectively. When the ADRC controls an object, the gain factors  $b_0$ ,  $g_0$ , and  $b_{0Dc}$  are tuned to obtain an acceptable and stable transient response.

However, though the conventional ADRC (Figure 1) extends to a new state variable ( $z_3$ ) to actively estimate and compensate for disturbances, it does not have the characteristics of compensating for these uncertainties in the presence of time delay.

In [19,20,33,35], the ADRC structure considered is commonly modified from the conventional ADRC, as illustrated in Figure 2. This modified structure comprises a time-delay block connected to one of the inputs of ESO (after the  $b_{0Dc}$  block seen in Figure 2). This will synchronize the signals entering the observer and enable it to effectively estimate the delayed system states and disturbances as the system’s output is already delayed according to the system dynamic. Thus, this feature can accommodate time-delay compensation [35].

In this paper, the ADRC method used for experimentations and comparisons in Section 4 is the modified time-delay-based ADRC shown in Figure 2. Time-delay blocks are added, one at the input fed to the ESO subsystem and the other at the output of the controlled object. The former delay block constitutes the delay to the input signal, whereas

the latter delay block (after the controlled object) is called the output delay and constitutes the system delay.

For the sake of simplicity, in this paper, the system to be controlled in Figure 2 is a linear controlled object, which is a second-order system represented by its state-space model given in Equation (10):

$$\begin{cases} \dot{x}(t) = Ax(t) + B(u(t) + \delta(x(t), t)) \\ y(t) = C^T x(t - \tau) + n(t), t \geq 0 \\ x(0) = [0 \ 0]^T \end{cases} \quad (10)$$

where  $x(t) = [x_1(t), x_2(t)]^T$  is the system state vector,  $n(t)$  is the measurement noise,  $u(t)$  is the control input,  $y(t)$  is the measured delayed output, and  $\tau$  is the time delay.  $\delta(x(t), t)$  and  $n(t)$  are the total disturbance and measurement noise acting on the system.  $\delta(x(t), t)$  includes unknown internal system dynamics due to delay, external disturbances, and measurement noise. Matrices  $A$ ,  $B$ , and  $C$  are the state transition matrix, input matrix, and output matrix of the plant, respectively.

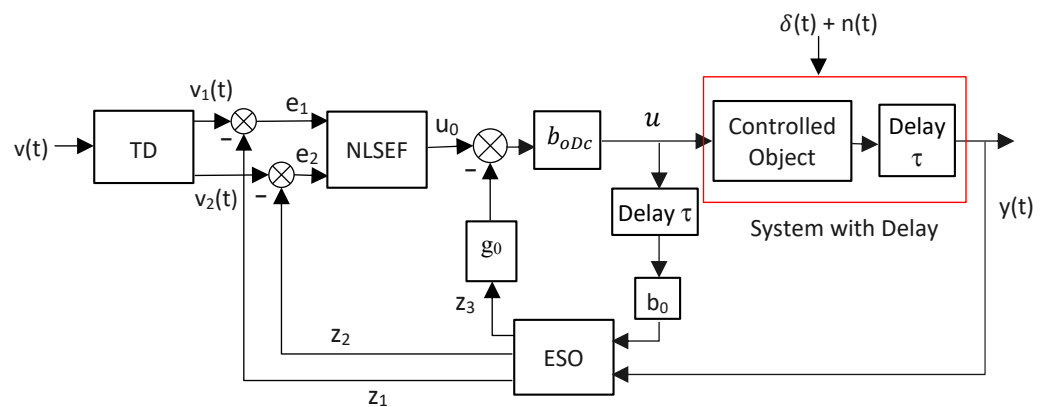


Figure 2. Modified time-delay-based ADRC structure for a given system.

### 2.2. ESPO-Based Controller

The ESPO-based controller is model-based contrary to the ADRC, which is a model-free controller. This controller shows a decent disturbance estimation and rejection for systems with sensor delay (measurement delay) by constructing an extended state for the predictor observer (PO) [29]. In an ESPO-based controller, the object to be controlled is a delayed system with uncertainties given in Equation (10).

The ESPO [29] heavily relies on the system model. When the system model is changed, the controller parameter “ $K$ ” is recalculated using the full state feedback pole assignment method, such that  $(A - BK^T)$ , for the system in Equation (10), provides a desired transient response (small rise time, zero SSE, less overshoot) at the desired eigenvalues. The ideal trajectory  $x^*(t)$  follows the signal  $x(t)$  and is given by Equation (11):

$$\begin{cases} \dot{x}^*(t) = Ax^*(t) - BK^T(x^*(t) - r(t)) \\ x^*(t_0) = x(t_0), t \in [t_0, \infty) \end{cases} \quad (11)$$

where  $t_0$  is the initial time and  $r(t)$  is the reference signal of  $x(t)$ .

The estimation and compensation of the total system disturbances by the extended state of the predictor observer are pictorially represented in Figure 3.

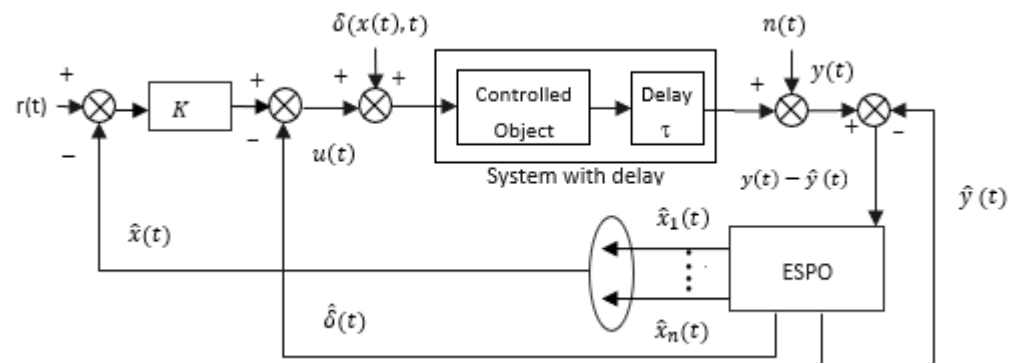


Figure 3. Extended state predictor observer (ESPO) mechanism.

The ESPO is designed using Equations (12)–(14):

$$\begin{bmatrix} \dot{\hat{x}}(t) \\ \dot{\hat{\delta}}(t) \end{bmatrix} = A_e \begin{bmatrix} \hat{x}(t) \\ \hat{\delta}(t) \end{bmatrix} + e^{A_e \tau} L_e (y(t) - \hat{y}(t)) + B_e u(t) \tag{12}$$

$$\hat{y}(t) = C_e^T \begin{bmatrix} \hat{x}(t - \tau) \\ \hat{\delta}(t - \tau) \end{bmatrix} + C_e^T \int_{t-\tau}^t e^{A_e(t-s)} L_e (y(s) - \hat{y}(s)) ds \tag{13}$$

where

$$\begin{cases} A_e = \begin{bmatrix} A & B \\ 0 & 0 \end{bmatrix}, B_e = \begin{bmatrix} B \\ 0 \end{bmatrix} \\ C_e = \begin{bmatrix} C \\ 0 \end{bmatrix}, L_e = \begin{bmatrix} 3\omega_e \\ 3\omega_e^2 \\ \omega_e^3 \end{bmatrix} \end{cases} \tag{14}$$

and the estimation of  $x(t)$  and  $\delta(x(t), t)$  is given as  $\hat{x}(t)$  and  $\hat{\delta}(t)$ , respectively.  $e^{A_e \tau}$  denotes the state transition matrix. The choice of the parameter matrix  $L_e$  is explained in Lemma 1.

**Lemma 1:** Let  $\omega_e$  be the ESPO bandwidth and the parameter vector  $L_e \in \mathbb{R}^{(n+1) \times 1}$  be the observer gain. The parameter  $L_e$  is tuned such that the matrix  $A_{L_e}$  in Equation (15) is Hurwitz stable.

$$A_{L_e} \triangleq A_e - L_e C_e^T \tag{15}$$

The individual ESPO gains  $l_i$  (for  $i = 1, 2, 3$ ) are selected such that  $L_e$  satisfies Equation (15); that is, the eigenvalues of the matrix  $(A_e - L_e C_e^T)$  when placed at  $-\omega_e$  give values of  $l_1 = 3\omega_e$ ,  $l_2 = 3\omega_e^2$ , and  $l_3 = \omega_e^3$ . This selection is performed as per the scaling and bandwidth parameterization technique seen in [43] and the pole placement technique [44]. Further, [45] gives an algorithm explaining the calculation of  $L_e$ . □.

The control law for the ESPO is given in Equation (16):

$$u(t) = -K^T (\hat{x}(t) - r(t)) - \hat{\delta}(t) \tag{16}$$

From the above equations, the disturbance  $\delta(t)$  is replaced by its estimate  $\hat{\delta}(t)$  that contains disturbances and other unknown dynamics. The  $A_e$  and  $B_e$  matrices indicate the variation of disturbance over time,  $e^{A_e \tau} L_e (y(t) - \hat{y}(t))$ , as per Equations (12)–(14). Expression  $y(t) - \hat{y}(t)$  represents the estimation error. Thus, ESPO estimates total disturbance in a time-delayed system and compensates for it in real time.

### 2.3. Integral of Time-Weighted Absolute Error (ITAE) Criterion

The ITAE criterion [46] given in Equation (17) is a commonly used performance index that gives the controller parameters with a reduced system error. The controller tuned in this context refers to the modified time-delay ADRC design in Figure 2. The parameters of

the delay-based ADRC were tuned using a genetic algorithm (GA) to minimize the ITAE (objective cost function).

$$ITAE = \int_0^{\infty} t|e(t)|dt \tag{17}$$

where  $t$  is the time and  $e(t)$  denotes the difference between the reference signal and controlled output.

#### 2.4. Optimizing the Controller Parameters using GA

The GA is an intelligent optimization algorithm that is used to find an optimal solution for a given problem by maximizing or minimizing a particular cost function. At every iteration, GA calculates the best  $f(x)$  value and the mean  $f(x)$  value of the specified fitness function, and these values are targeted to be minimized in each successive generation [47,48]. In this paper, GA optimization is performed offline to find the optimal parameters of the delay-based ADRC shown in Figure 2. The steps followed during the GA optimization are presented in a flowchart shown in Figure 4.

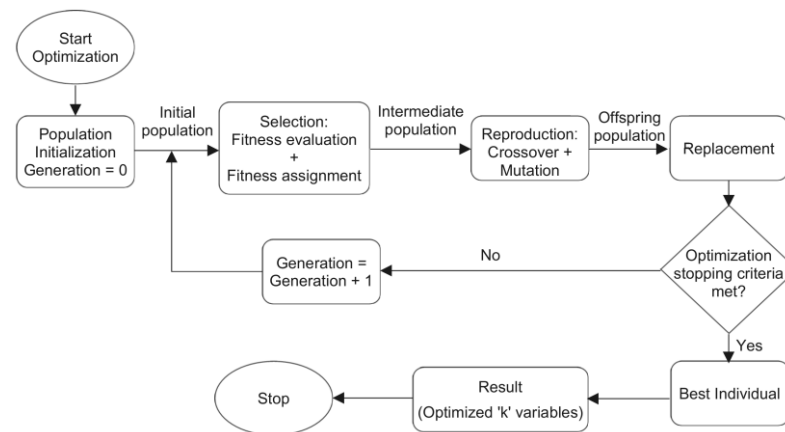


Figure 4. Typical genetic algorithm (GA) flowchart.

### 3. Proposed Predictive ESO-based Active Disturbance Rejection Control Design

The novel controller design (called the predictive ESO-based ADRC) proposed in this paper combines the advantages of both the ADRC and ESPO-based controllers, as shown in Figure 5. In the proposed method, ADRC contributes to the transient profile generation, the nonlinear state error feedback control, and the total disturbance estimation and compensation. To be more specific, the ADRC uses TD for fast input tracking, and in turn, the outputs of TD are fed to the NLSEF, which is used to reduce the SSE significantly and to reach a zero steady state faster in a finite time.

Time-delay blocks are present in the proposed method. As seen in Figure 5, one is at the inputs of the ESO, and the other is at the plant’s output.

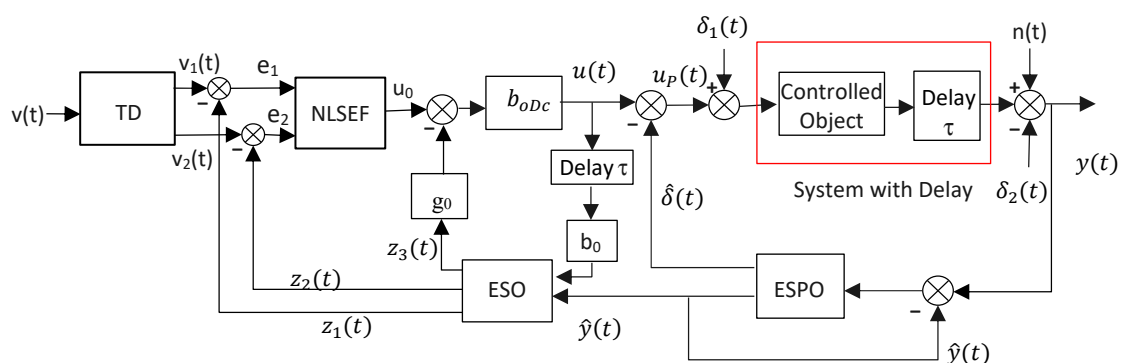


Figure 5. Proposed predictive ESO-based ADRC structure.

The ESPO-based controller's operation seen in Figure 5 is designed using the set of Equations (11)–(14). ESPO estimates the total disturbance which is contributed by all factors (unknown dynamics due to delay, external disturbance, and noise). The estimated total disturbance given by  $\hat{\delta}(t)$  is compensated by removing it from the control input signal  $u(t)$ , seen in Equation (19) and Figure 5. This  $\hat{\delta}(t)$  can be obtained from Equation (12) and is inclusive of the external disturbances and unknown system dynamics generated during the delay. In addition, from Figure 5, the variation of  $\hat{\delta}(t)$  depends on the estimation error that is indicated by the difference between plant output and the ESPO predicted output, " $y(t) - \hat{y}(t)$ ".

The delayed control input  $u(t)$  and the ESPO predicted output  $\hat{y}(t)$  are fed to the ESO. In the proposed controller design, instead of feeding the plant output  $y(t)$  to the ADRC's ESO (which is not available due to the time-delay and output disturbances present), the predicted output  $\hat{y}(t)$  from the ESPO is fed to the ESO.

The system or object to be controlled by the proposed controller is specified in Equation (18):

$$\begin{cases} \dot{x}(t) = Ax(t) + B(u_P(t) + \delta_1(x(t), t)) \\ y(t) = C^T x(t - \tau) + \delta_2(x(t), t) + n(t) \end{cases} \quad (18)$$

where  $x(t) = [x_1(t), x_2(t)]^T$ ,  $u_P(t)$ ,  $y(t)$ , and  $\tau$  are the system state vector, control input, measured output, and time delay, respectively. Matrices,  $A$ ,  $B$ , and  $C$  are the state transition matrix, input matrix, and output matrix of the plant.  $\delta_1(x(t), t)$  and  $\delta_2(x(t), t)$  correspond to the input and output disturbances present in the system. The measurement noise  $n(t)$  in Figure 5 is a sequence of the white noise signal.

The control law  $u_P(t)$  for the proposed controller design is given by Equation (19):

$$\begin{cases} u_P(t) = u(t) - \hat{\delta}(t) \\ u_P(t) = (u_0(t) - z_3 g_0) b_{0Dc} - \hat{\delta}(t) \\ u_P(t) = (-fhan(e_1, c \cdot e_2, r, h_1) - z_3 g_0) b_{0Dc} - \hat{\delta}(t) \end{cases} \quad (19)$$

The novel ESO algorithm of the proposed controller is given in Equation (20):

$$\begin{cases} e = z_1 - \hat{y} \\ \dot{z}_1 = z_2 - \beta_{01} e \\ \dot{z}_2 = z_3 - \beta_{02} f e + b_0 u(t - \tau) \\ \dot{z}_3 = -\beta_{03} f e_1 \end{cases} \quad (20)$$

where  $g_0$  and  $b_0$  are the gain factors and  $b_{0Dc}$  is the disturbance compensation factor.  $\beta_{01}$ ,  $\beta_{02}$ , and  $\beta_{03}$  are the ESO gains.  $r$  and  $h_1$  are control gain and precision factors of the NLSEF. Functions  $fhan$ ,  $f e$ , and  $f e_1$  are the nonlinear functions given in Equations (5) and (8). The remaining parameters used in Equations (19) and (20) are defined in Section 2.1 (Conventional ADRC) of this paper.

The objects or systems with delay to be controlled by the proposed controller design include the second-order Type 0, Type 1, and Type 2 systems. The transfer functions and state-space representations for all the systems are given in Section 4. It was observed that the Type 1 and Type 2 systems are more challenging to control because their dynamics are usually more aggressive than those of the Type 0 systems. Thus, in the experiments for the Type 0 system, a GA algorithm could optimize six parameters ( $c$ ,  $h_1$ ,  $r$ ,  $g_0$ ,  $b_0$ , and  $b_{0Dc}$ ) of the modified time-delay-based ADRC structure seen in Figure 2. However, only three parameters ( $c$ ,  $h_1$ , and  $r$ ) could be optimized for Type 1 and Type 2 systems, with the other three parameters ( $g_0$ ,  $b_0$ , and  $b_{0Dc}$ ) being manually determined.

The control strategy of the novel proposed controller method, obtained by cascading the delay-based ADRC with ESPO-based controllers, is shown in an algorithmic procedure shown in Algorithm 1.

**Algorithm 1.** Control Design of the Proposed Predictive ESO-based ADRC Controller

---

Design the controller NLSEF of the modified time-delay-based ADRC structure: Use GA to find the optimal damping coefficient  $c$ , the precision factor  $h_1$ , and the control gain  $r$  that minimizes the ITAE between the output response and the desired response. An automatic stop condition is incorporated. The optimization is conducted using the GA for Type 0 system given bounds on  $c, h_1, r, g_0, b_0,$  and  $b_{0Dc}$  for a time-delay  $\tau$ , whereas the optimization is conducted using the GA for Type 1 and Type 2 systems given bounds on  $c, h_1,$  and  $r$  for a time-delay  $\tau$ .  $\beta_{01}, \beta_{02}, \beta_{03},$  and  $h_{ESO}$  for the ESO are kept constant.  $h$  and  $r_0$  for TD are kept constant.

1:       if  $c, h_1, r, g_0, b_0,$  or  $b_{0Dc}$  (for Type 0) value or  $c, h_1,$  or  $r$  (for Type 1 and Type 2 systems) value falls on the bound after an optimization run  
       then  
 2:           bounds are changed and the ADRC is re-optimized.  
 3:       Else  
 4:           Save the best  $c, h_1, r, g_0, b_0,$  and  $b_{0Dc}$  (for Type 0) or  $c, h_1,$  and  $r$  (for Type 1 and Type 2 systems).  
 5:       end if

6:       Design the observer ESPO: Use Equations (11)–(14). The bandwidth  $\omega_e$  is tuned to obtain the best disturbance compensation performance, given the input disturbances  $\delta_1(t)$  and output disturbance  $\delta_2(t)$ .

7:       Obtain the control law ( $u_p(t)$ ) of the proposed controller design using Equation (19). Simulate, with time-delay  $\tau$ , the control of the plant by the proposed predictive ESO-based ADRC: The aim is to assess the proposed design's controller performance for disturbance compensation in the presence of time delay. Keep the constants of ESPO found in line 7, delay-based ADRC constants, and NLSEF parameters found through the optimization in line 2 of Algorithm 1, with the input disturbances  $\delta_1(t)$  and output disturbance  $\delta_2(t)$ , and measurement noise  $n(t)$ .

---

**4. Experiments and Results**

This section presents the results of experiments wherein the proposed controller (predictive ESO-based ADRC) is compared with the modified delay-based ADRC and ESPO-based controller methods. First, the different controllers are simulated with time-delay  $\tau$ , to control each plant type (Type 0, Type 1, and Type 2 system) individually. This is followed by assessing the respective controller performances for disturbance compensation in presence of delay, given the input disturbances  $\delta_1(t)$ , output disturbance  $\delta_2(t)$ , and noise  $n(t)$ , because different system types challenge a controller differently.

As shown in Figure 5, the proposed predictive ESO-based ADRC design is composed of two control methods integrated: (1) modified time-delay-based ADRC structure and (2) ESPO-based controller. The choice of parameters for each is explained in the following text:

## (1) Modified time-delay-based ADRC:

The modified ADRC system given in Figure 2 was optimized using GA, as explained in line 1 of Algorithm 1. The GA optimization was performed offline, using the Optimization Tool Window in MATLAB version R2020a. To perform GA optimization to find an optimal parameter set of the modified delay-based ADRC structure (in Figure 2), the following stopping criteria were used: number of generations = 100 times the number of variables, stall generation = 50, function tolerance =  $1 \times 10^{-6}$ , and constraint tolerance =  $1 \times 10^{-3}$ . When optimizing, the stop time of all Simulink models was set to 80 s.

Table 1 lists the ADRC parameter values  $k = [c, h_1, r, g_0, b_0, b_{0Dc}]$  that were optimized for the Type 0 system. For Type 1 and Type 2 systems, three of the ADRC parameter values  $k = [c, h_1, r]$  were optimized. The remaining ADRC values were kept fixed:  $r_0 = 10$  and  $h = 0.03$  for the TD subsystem and  $\beta_{01} = 100, \beta_{02} = 300, \beta_{03} = 1000,$  and  $h_{ESO} = 0.01$  for the ESO subsystem were taken from [40]. ESO gains ( $\beta_{01}, \beta_{02},$  and  $\beta_{03}$ ) have no predetermined values and can be chosen in many ways depending on a certain problem. For instance, to

calculate the ESO gains, different relations in connection with  $h_{ESO}$  (ESO step size) have been given in [7]. Therefore, for an ADRC, the important parameters to be tuned are the damping coefficient ( $c$ , to be regulated around unity), precision coefficient ( $h_1$ , is usually at least 4 times the sampling period  $h$ ), amplification coefficient ( $r$ ), and gain/compensation factors ( $b_0$ ) [7,40]. Hence, these parameters were optimized to obtain an appropriate performance in terms of transient response, and steady state, for the system concerned.

Further,  $g_0$  and  $b_{0Dc}$  are the gain factor and disturbance compensation factor, respectively. When the ADRC controls the Type 0 system, the gain factors  $b_0$ ,  $g_0$ , and  $b_{0Dc}$  are also tuned to obtain an acceptable and stable transient response. However, for Type 1 and Type 2 systems, the gain factors were set to unity. It is important to note that Type 1 and Type 2 systems are more difficult to control as their dynamics are more aggressive; thus, more parameters could be controlled (optimized) for the Type 0 system.

**Table 1.** ADRC parameter values of the proposed controller design.

Delay-Based ADRC	$c$	$h_1$	$r$	$g_0$	$b_0$	$b_{0Dc}$
Type 0 System	0.7645	1.0831	56.0350	0.3097	3.1303	1.0314
Type 1 System	1.0710	0.9340	41.5480	1.0000	1.0000	1.0000
Type 2 System	0.8990	2.0216	62.9887	1.0000	1.0000	1.0000

(2) ESPO-based controller:

ESPO was designed for each system using Equations (11)–(14). The reference signal  $r(t)$  seen in Equation (16) is set to  $[1 \ 0]^T$ . Each system has specific  $K$  values, with which the desired real eigenvalues satisfying the transient response and SSE are obtained. The following  $K$  values were obtained for each system type, at which the fastest stable response with no overshoot and having a unit gain was obtained:  $K = [49/72 \ -1/3]$  for the Type 0 system (seen in Equations (23) and (24)),  $K = [1/4 \ 0]$  for the Type 1 system (given in Equations (25) and (26)), and  $K = [4 \ 4]$  for the Type 2 system (provided in Equations (27) and (28)).

To agree with the ESPO-based controller’s [29] method for comparison, the ESPO bandwidth ( $\omega_e = 5$ ) and time delay ( $\tau = 0.1$  s) for the proposed controller are kept the same in Sections 4.1–4.4. When studying the time-delay effect,  $\tau$  is varied in Section 4.5. The state-space model of each system is represented using the form in Equation (18).

In the proposed controller structure (proposed predictive ESO-based ADRC) seen in Figure 5, it must be noted that the reference input signal  $v(t)$  to TD of ADRC was a step signal with a final unity value applied at  $t = 0$  s. The input disturbance  $\delta_1(t)$  is added after 20 s, while output disturbance  $\delta_2(t)$  starts from the 40th second. The input disturbance  $\delta_1(x(t), t)$  and step output disturbance  $\delta_2(x(t), t)$  seen in Equation (18) are given by Equations (21) and (22), respectively. In addition, the measurement noise  $n(t)$  is a sequence of white noise signals having a standard deviation of 0.005, as seen in [29].

$$\begin{cases} C_1 : \delta_1(x(t), t) = 0 \\ C_2 : \delta_1(x(t), t) = 0.4 \sin(x_1) - 0.1u + 0.2 \sin(\frac{\pi}{8t}) \\ C_3 : \delta_1(x(t), t) = -0.2e^{\cos x_2} + 0.1u + 0.2 \operatorname{sign}(\sin(\frac{\pi}{8t})) \\ C_4 : \delta_1(x(t), t) = 0.1x_2 + \min\left\{1, \max\left\{\frac{t-5}{5, 0}\right\}\right\} \\ C_5 : \delta_1(x(t), t) = 0.3 \operatorname{step}(t - \theta) \end{cases} \tag{21}$$

$$\delta_2(x(t), t) = 0.3 \operatorname{step}(t - \theta) \tag{22}$$

In this study, different performance criteria have been tabulated, including the ITAE corresponding to the durations in which input disturbance (at 20 s) and step output disturbance (at 40 s) are applied. Additionally, the transient response characteristics are also displayed, including the overshoot at startup from reference (OS, %), rise time ( $T_r$ , s), the maximum deviation from the reference due to input disturbance ( $D_{m,i}$ ), the maximum drop from the reference due to output disturbance ( $d_{m,o}$ ), and the adjustment time to return to reference after output disturbance is applied ( $T_a$ , s). Furthermore, discussions on disturbance compensation capability (depression width) and suppression of initial overshoot due to time delay present are also provided. Thus, these transient response characteristics will serve as a measure for interpreting the transparency of these systems controlled by the proposed method.

#### 4.1. Experiment 1: Second-Order Type 0 System

The Type 0 system studied in this experiment is represented by its transfer function and state-space model in Equations (23) and (24), respectively.

$$G_{Type0}(s) = \frac{2}{s^2 + 3s + 2} e^{-\tau s}; \tau = 0.1s \quad (23)$$

$$\begin{cases} \dot{x} = Ax + Bu \\ y = Cx(t - \tau) \\ \text{where } A = \begin{bmatrix} -3 & 1 \\ -2 & 0 \end{bmatrix}, B = \begin{bmatrix} 0 \\ 2 \end{bmatrix}, C = [1 \ 0] \end{cases} \quad (24)$$

The responses for the controlled second-order Type 0 system are shown in Figures 6 and 7, respectively. For the cases of input disturbance only and both input disturbance and step output disturbance included, under time-delay control, performance index criteria are summarized in Tables 2 and 3.

The following key observations are inferred from Tables 2 and 3 for the performance index values for the Type 0 system under various scenarios:

1. The values of the maximum drop from reference ( $d_{m,o}$ ) due to output disturbance are similar for all methods, but the adjustment time needed to return to reference ( $T_a$ ) is small for the proposed design compared with the delay-based ADRC (refer to Table 3). For the ESPO method, the response curve does not attain zero SSE after output disturbance compensation (refer to Figure 7a,d,e).
2. As shown in Table 2, in the case of both disturbances present, i.e., input ( $C_2$ ) and step output disturbances, the proposed system gives the smallest ITAE values of 3.4517 (from 0 s to 40 s), 19.0940 (from 40 s to 80 s), and 22.5330 (from 0 s to 80 s), whereas the corresponding ITAE values for ADRC and ESPO are relatively higher.
3. A comparison of the rise time ( $T_r$ ) values in Table 3 shows that the considered ADRC and the proposed method had similar readings, unlike high rise times such as 3.0323 s and 2.5485 s as seen for the ESPO design. Further, for the proposed method, in Figure 7b,d, the overshoot (OS) at the beginning of the response curve due to the time delay present is reduced by about 1% and 3.6% when compared to that of the delay-based ADRC.
4. Thus, it is shown from Figures 6 and 7 that the proposed method presented for the Type 0 system performed more robustly when compensating both the input and step output disturbances with noise in the presence of time delay, as compared to the modified time-delay-based ADRC and ESPO methods.

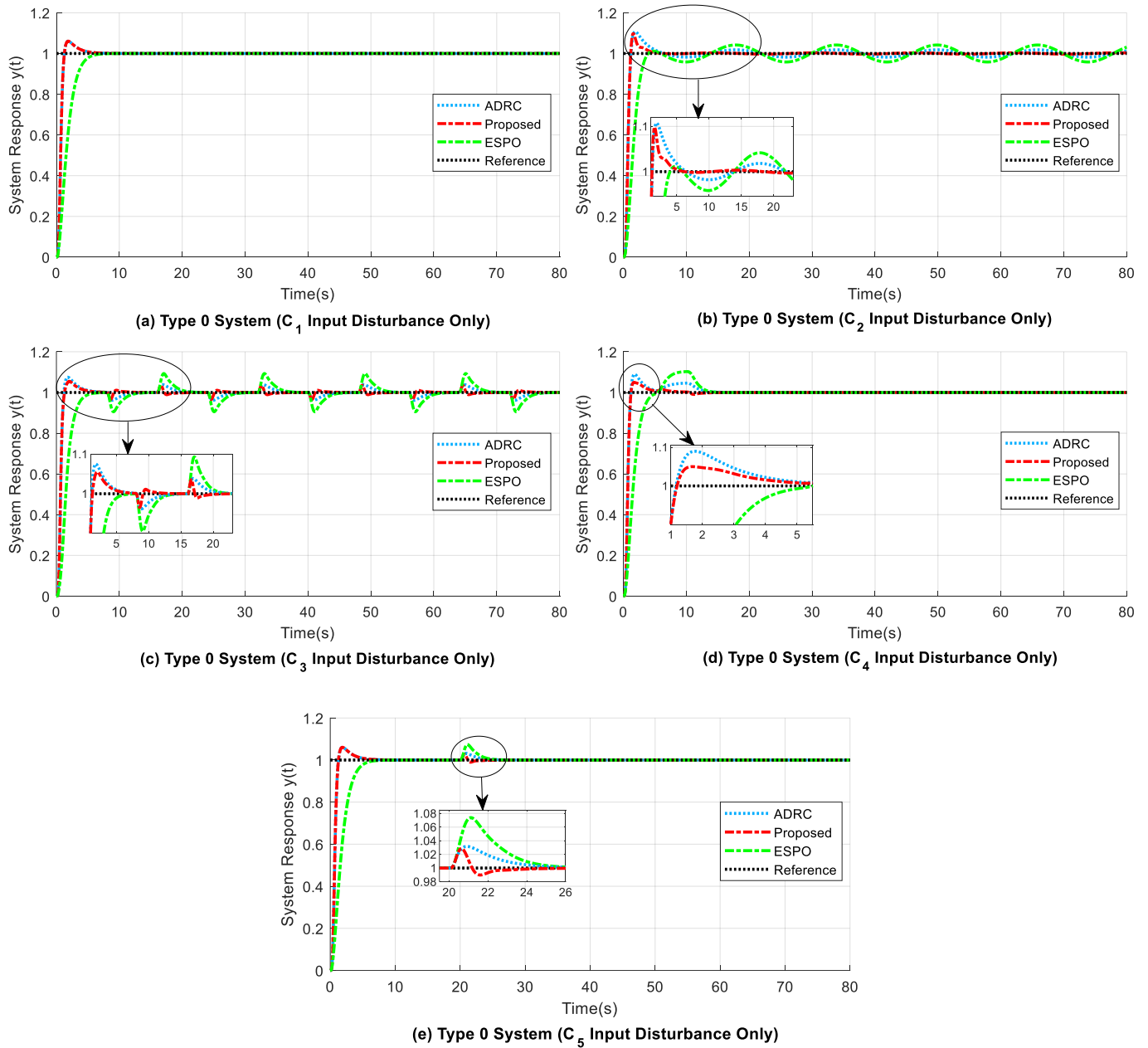


**Figure 6.** Responses for the case of only input disturbances are presented for the Type 0 system: (a) only  $C_1$  input disturbance present; (b) only  $C_2$  input disturbance present; (c) only  $C_3$  input disturbance present; (d) only  $C_4$  input disturbance present; (e) only  $C_5$  input disturbance present.

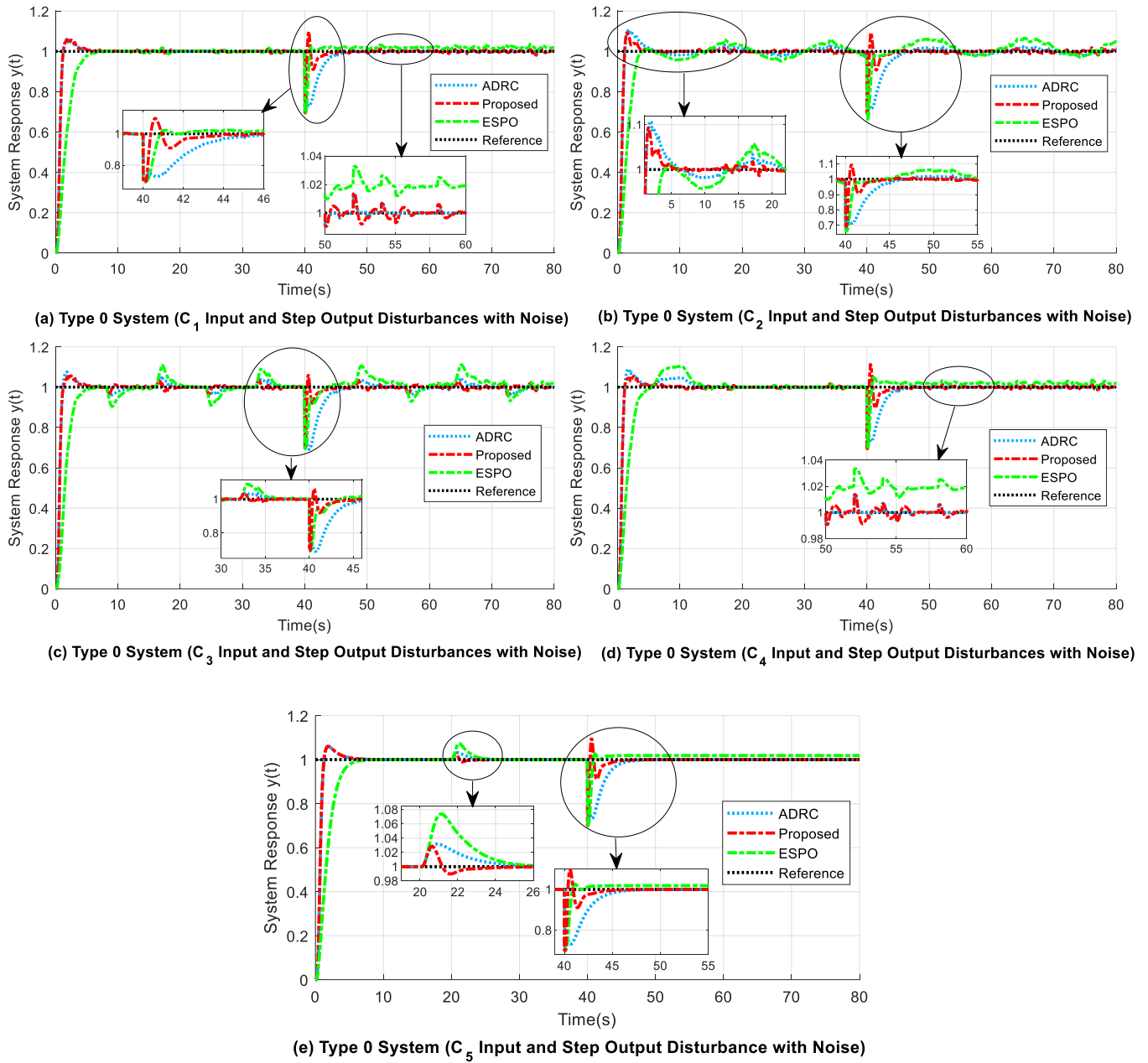


**Figure 7.** Responses for the different input disturbances and step output disturbance with noise for the Type 0 system: (a)  $C_1$  of  $\delta_1(x(t), t)$ ,  $\delta_2(x(t), t)$ , and noise present; (b)  $C_2$  of  $\delta_1(x(t), t)$ ,  $\delta_2(x(t), t)$ , and noise present; (c)  $C_3$  of  $\delta_1(x(t), t)$ ,  $\delta_2(x(t), t)$ , and noise present; (d)  $C_4$  of  $\delta_1(x(t), t)$ ,  $\delta_2(x(t), t)$ , and noise present; (e)  $C_5$  of  $\delta_1(x(t), t)$ ,  $\delta_2(x(t), t)$ , and noise present.

**Table 2.** ITAE performance index values for Type 0 system.

Input Disturbance Number	Method	With Input Disturbance ( $C_i$ ) *			With Input Disturbance ( $C_i$ ) *, Output Disturbance, and Noise		
		ITAE (0–40 s)	ITAE (40–80 s)	ITAE (0–80 s)	ITAE (0–40 s)	ITAE (40–80 s)	ITAE (0–80 s)
$i = 1$	ADRC	0.6676	0.0009	1.0607	<b>1.6124</b>	31.1490	32.7500
	Proposed	<b>0.6676</b>	0.0009	<b>0.6685</b>	2.5574	<b>17.4630</b>	<b>20.0080</b>
	ESPO	2.3805	$\approx 0$	2.3805	4.3932	50.4860	54.8670
$i = 2$	ADRC	9.6014	27.387	36.988	9.7792	53.7620	63.5280
	Proposed	<b>2.25885</b>	<b>5.1091</b>	<b>7.3678</b>	<b>3.4517</b>	<b>19.0940</b>	<b>22.5330</b>
	ESPO	21.6490	62.9280	84.5760	21.2200	72.2790	93.4850
$i = 3$	ADRC	8.2367	24.8410	33.0780	8.6993	53.2740	61.9610
	Proposed	<b>3.8284</b>	<b>10.7540</b>	<b>14.5830</b>	<b>4.6495</b>	<b>21.6770</b>	<b>26.3140</b>
	ESPO	18.3780	54.2800	72.6580	18.8440	77.7070	96.5380
$i = 4$	ADRC	3.0302	0.0003	3.0304	3.9263	30.2750	34.1890
	Proposed	<b>1.0168</b>	0.0009	<b>1.0177</b>	<b>2.9576</b>	<b>18.5780</b>	<b>21.5230</b>
	ESPO	6.6778	$\approx 0$	6.6778	8.6929	52.2850	60.9650
$i = 5$	ADRC	2.2397	0.0006	2.2403	<b>3.1505</b>	31.1490	34.2880
	Proposed	<b>1.3506</b>	0.0009	<b>1.3515</b>	3.1726	<b>17.4630</b>	<b>20.6230</b>
	ESPO	5.7809	$4.7184 \times 10^{-6}$	5.7809	7.7430	50.4860	58.2160

\*  $C_i$  is input disturbance that corresponds to input disturbance number  $i$  ( $C_1, C_2, C_3, C_4, C_5$  of  $\delta_1(x(t), t)$ ).

**Table 3.** Other performance index values for Type 0 system.

Input Disturbance Number	Method	With Input Disturbance ( $C_i$ ) *			With Input Disturbance ( $C_i$ ) *, Output Disturbance, and Noise			
		OS (%)	$T_r$ (s)	$D_{m,i}$	OS (%)	$T_r$ (s)	$d_{m,o}$	$T_a$ (s)
$i = 1$	ADRC	6.0700	0.6478	$\approx 0$	6.0700	0.6298	<b>0.2721</b>	8.0300
	Proposed	6.0700	<b>0.6478</b>	$\approx 0$	5.8200	<b>0.6308</b>	0.3051	<b>5.6500</b>
	ESPO	$\approx 0$	2.8782	$\approx 0$	<b>0.7200</b>	3.0323	0.3051	Non-zero finite SSE
$i = 2$	ADRC	10.7500	0.6459	0.0182	10.7300	0.6299	0.3190	7.0600
	Proposed	9.8400	<b>0.6121</b>	<b>0.0031</b>	9.3800	<b>0.6002</b>	<b>0.3085</b>	5.3800
	ESPO	<b>1.8300</b>	2.4102	0.0418	<b>1.8400</b>	2.4449	0.3374	<b>4.2400</b>
$i = 3$	ADRC	7.5100	0.5966	0.0387	7.5200	0.5943	0.3088	8.1700
	Proposed	5.4900	<b>0.5982</b>	<b>0.0358</b>	5.6300	<b>0.5960</b>	<b>0.3052</b>	5.5500
	ESPO	$\approx 0$	2.3637	0.0946	<b>0.4800</b>	2.3880	0.3052	<b>3.2300</b>
$i = 4$	ADRC	8.9500	0.6075	0.0030	8.9000	0.6019	<b>0.2678</b>	9.0200
	Proposed	8.9500	<b>0.6075</b>	<b>0.0030</b>	<b>5.2100</b>	<b>0.6060</b>	0.3056	<b>5.7200</b>
	ESPO	<b>1.0270</b>	2.5169	0.1030	10.4200	2.5485	0.3056	Non-zero finite SSE
$i = 5$	ADRC	6.0700	0.6478	0.0320	6.0700	0.6298	0.3051	8.0100
	Proposed	<b>6.0700</b>	<b>0.6478</b>	<b>0.0290</b>	5.8200	<b>0.6308</b>	<b>0.3057</b>	<b>5.5000</b>
	ESPO	7.3900	2.8782	0.0740	<b>0.7200</b>	3.0323	0.3000	Non-zero finite SSE

\*  $C_i$  is input disturbance that corresponds to input disturbance number  $i$  ( $C_1, C_2, C_3, C_4, C_5$  of  $\delta_1(x(t), t)$ ).

#### 4.2. Experiment 2: Second-Order Type 1 System

The transfer function and state-space representation of the second-order Type 1 system experimented with are given by Equations (25) and (26), respectively.

$$G_{Type1}(s) = \frac{1}{s^2 + s} e^{-\tau s}; \tau = 0.1s \tag{25}$$

$$\begin{cases} \dot{x} = Ax + Bu \\ y = Cx(t - \tau) \end{cases} \tag{26}$$

where  $A = \begin{bmatrix} -1 & 1 \\ 0 & 0 \end{bmatrix}$ ,  $B = \begin{bmatrix} 0 \\ 1 \end{bmatrix}$ ,  $C = [1 \ 0]$

Figures 8 and 9 show the responses obtained for the Type 1 system for the cases of input disturbance only ( $C_1, C_2, C_3, C_4, C_5$ ), and input disturbance and step output disturbance are both included under the time-delay scenario. Performance index criteria are reported in Tables 4 and 5.

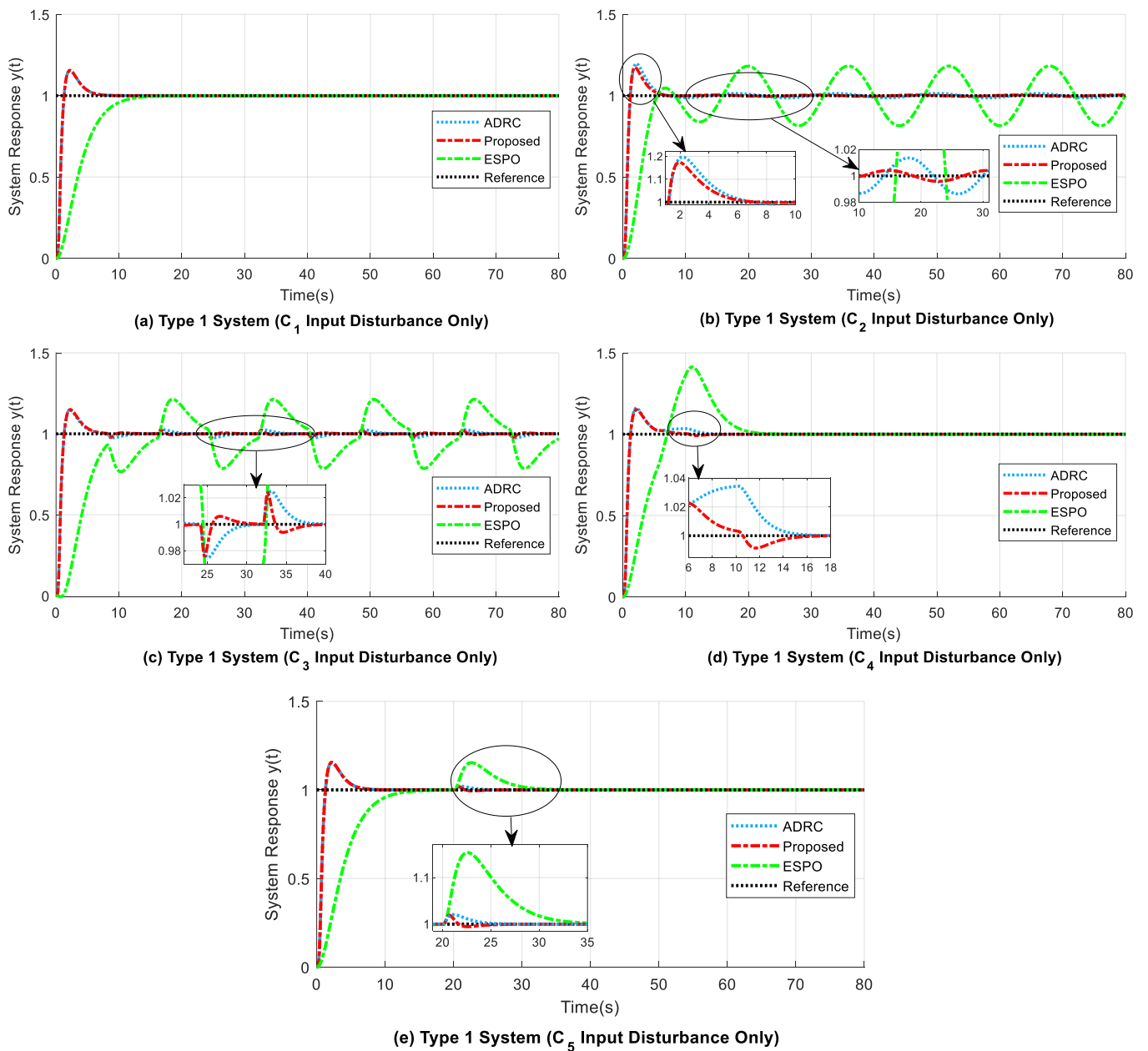


**Figure 8.** Responses for the case of only input disturbances are presented for the Type 1 system: (a) only  $C_1$  input disturbance present; (b) only  $C_2$  input disturbance present; (c) only  $C_3$  input disturbance present; (d) only  $C_4$  input disturbance present; (e) only  $C_5$  input disturbance present.

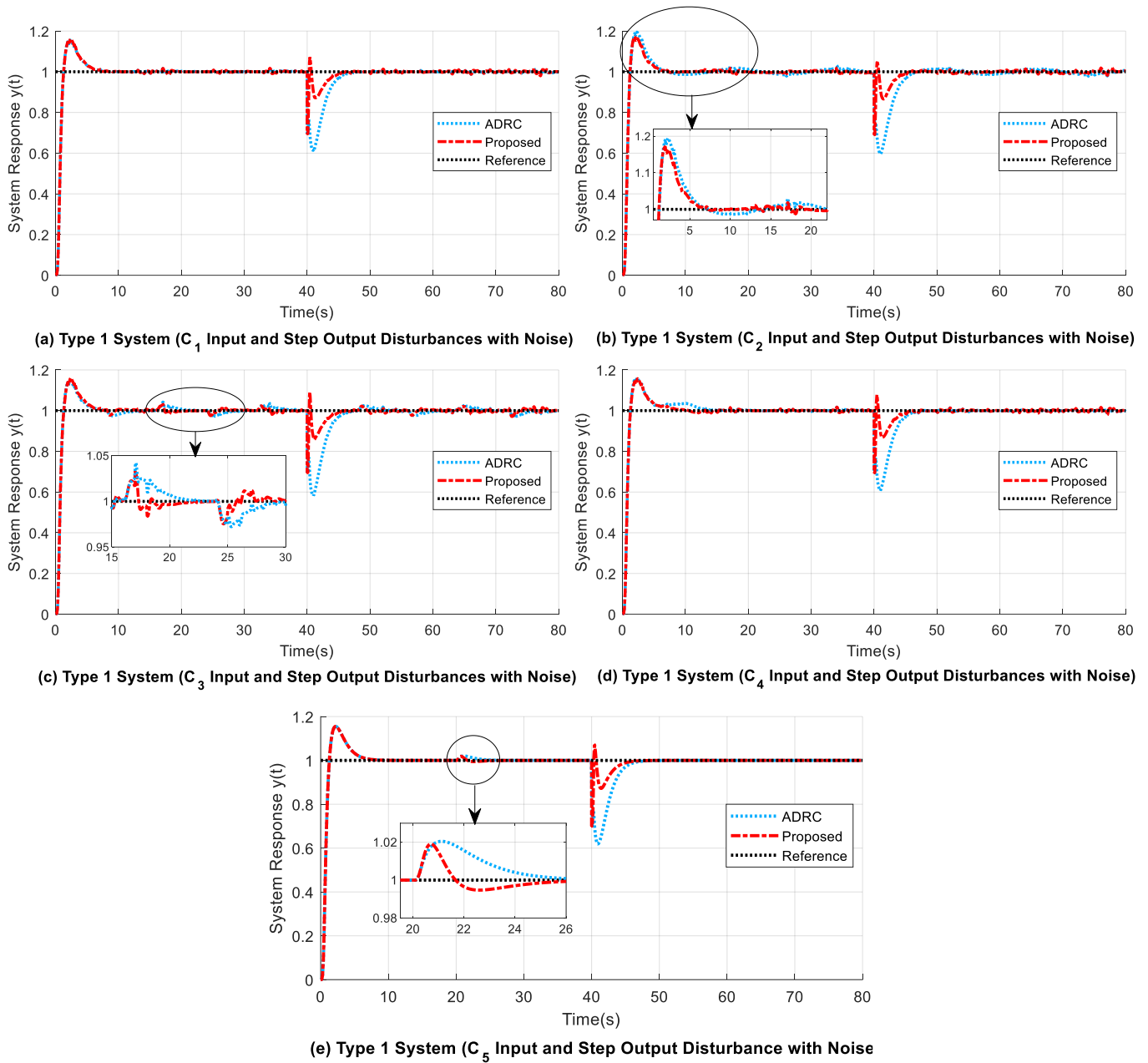


**Figure 9.** Responses for the different input disturbances and step output disturbance with noise for the Type 1 system: (a)  $C_1$  of  $\delta_1(x(t), t)$ ,  $\delta_2(x(t), t)$ , and noise present; (b)  $C_2$  of  $\delta_1(x(t), t)$ ,  $\delta_2(x(t), t)$ , and noise present; (c)  $C_3$  of  $\delta_1(x(t), t)$ ,  $\delta_2(x(t), t)$ , and noise present; (d)  $C_4$  of  $\delta_1(x(t), t)$ ,  $\delta_2(x(t), t)$ , and noise present; (e)  $C_5$  of  $\delta_1(x(t), t)$ ,  $\delta_2(x(t), t)$ , and noise present.

**Table 4.** ITAE performance index values for Type 1 system.

Input Disturbance Number	Method	With Input Disturbance ( $C_i$ ) *			With Input Disturbance ( $C_i$ ) *, Output Disturbance, and Noise		
		ITAE (0–40 s)	ITAE (40–80 s)	ITAE (0–80 s)	ITAE (0–40 s)	ITAE (40–80 s)	ITAE (0–80 s)
$i = 1$	ADRC	1.5766	$9.8378 \times 10^{-11}$	1.5766	<b>2.8122</b>	47.5200	50.3200
	Proposed	<b>1.5766</b>	<b><math>9.8378 \times 10^{-11}</math></b>	<b>1.5766</b>	3.3515	<b>22.6150</b>	<b>25.9540</b>
	ESPO	12.4050	$4.0049 \times 10^{-6}$	12.4050	Unstable	Unstable	Unstable
$i = 2$	ADRC	8.2185	20.4950	28.7130	8.9441	62.972	71.903
	Proposed	<b>3.4850</b>	<b>6.3879</b>	<b>9.8729</b>	<b>4.4819</b>	<b>24.3140</b>	<b>28.7830</b>
	ESPO	93.1820	280.2800	373.4600	Unstable	Unstable	Unstable
$i = 3$	ADRC	7.0513	18.5120	25.5630	7.8534	63.0580	70.8990
	Proposed	<b>4.6276</b>	<b>10.1540</b>	<b>14.7820</b>	<b>5.3395</b>	<b>28.0510</b>	<b>33.3780</b>
	ESPO	102.6800	284.4000	387.0800	Unstable	Unstable	Unstable
$i = 4$	ADRC	3.2785	$1.1437 \times 10^{-10}$	3.2785	4.4735	47.4000	51.8610
	Proposed	<b>2.0698</b>	$1.3578 \times 10^{-10}$	<b>2.0698</b>	<b>3.7814</b>	<b>22.9790</b>	<b>26.7480</b>
	ESPO	38.9340	0.0006	38.9340	Unstable	Unstable	Unstable
$i = 5$	ADRC	2.7463	$2.2000 \times 10^{-7}$	2.7463	3.9124	47.5200	51.4200
	Proposed	<b>2.2268</b>	<b><math>2.0090 \times 10^{-7}</math></b>	<b>2.2268</b>	<b>3.9120</b>	<b>22.6150</b>	<b>26.5150</b>
	ESPO	33.1020	0.0229	33.1250	Unstable	Unstable	Unstable

\*  $C_i$  is input disturbance that corresponds to input disturbance number  $i$  ( $C_1, C_2, C_3, C_4, C_5$  of  $\delta_1(x(t), t)$ ).

**Table 5.** Other performance index values for Type 1 system.

Input Disturbance Number	Method	With Input Disturbance ( $C_i$ ) *			With Input Disturbance ( $C_i$ ) *, Output Disturbance, and Noise			
		OS (%)	$T_r$ (s)	$D_{m,i}$	OS (%)	$T_r$ (s)	$d_{m,o}$	$T_a$ (s)
$i = 1$	ADRC	15.5500	0.6940	$\approx 0$	<b>15.5800</b>	<b>0.6750</b>	0.3903	9.0100
	Proposed	15.5500	<b>0.6940</b>	$\approx 0$	16.1500	0.6771	<b>0.3054</b>	<b>9.0100</b>
	ESPO	$\approx 0$	6.7158	$\approx 0$	Unstable	Unstable	Unstable	Unstable
$i = 2$	ADRC	19.7100	0.6767	0.0140	19.4800	0.6596	0.4049	7.0000
	Proposed	17.3800	<b>0.6534</b>	<b>0.0041</b>	<b>17.1600</b>	<b>0.6399</b>	<b>0.3095</b>	<b>7.0000</b>
	ESPO	<b>4.7300</b>	3.5289	0.1847	Unstable	Unstable	Unstable	Unstable
$i = 3$	ADRC	14.6700	<b>0.6884</b>	0.0250	<b>14.8900</b>	<b>0.6691</b>	0.4173	8.0400
	Proposed	15.0200	0.6991	<b>0.0242</b>	16.0800	0.6803	<b>0.3054</b>	<b>8.0400</b>
	ESPO	$\approx 0$	5.1066	0.2147	Unstable	Unstable	Unstable	Unstable
$i = 4$	ADRC	16.1500	0.6781	0.0340	16.1200	0.6598	0.3916	8.0000
	Proposed	<b>15.1300</b>	<b>0.6789</b>	<b>0.0086</b>	<b>15.7500</b>	0.6622	<b>0.3055</b>	<b>8.0000</b>
	ESPO	41.4200	5.2571	0.4140	Unstable	Unstable	Unstable	Unstable
$i = 5$	ADRC	15.5500	0.6940	0.0200	<b>15.5800</b>	<b>0.6750</b>	0.3899	8.0000
	Proposed	<b>15.5500</b>	<b>0.6940</b>	<b>0.0190</b>	16.1500	0.6771	<b>0.3055</b>	<b>7.3200</b>
	ESPO	15.3600	6.7158	0.1540	Unstable	Unstable	Unstable	Unstable

\*  $C_i$  is input disturbance that corresponds to input disturbance number  $i$  ( $C_1, C_2, C_3, C_4, C_5$  of  $\delta_1(x(t), t)$ ).

The following key results are obtained from Tables 4 and 5 based on the performance index values for the Type 1 system under different scenarios:

1. The maximum drop from reference due to output disturbance ( $d_{m,o}$ ) is slightly small for the proposed design when compared with that of the modified ADRC. However, the adjustment time needed to return to reference ( $T_a$ ) is similar for both the former and latter methods. The ESPO method is found to be unstable due to the application of step output disturbance at 40 s (refer to Table 5).
2. For input ( $C_2$ ) and step output disturbances present, the proposed system gives smaller ITAE values of 4.4819 (from 0 s to 40 s), 24.3140 (from 40 s to 80 s), and 28.7830 (from 0 s to 80 s). The corresponding ITAE values for ADRC are relatively higher, and the ESPO shows unstable behaviour due to step output disturbance.
3. For the proposed method, in Figures 8b and 9b, the overshoot (OS) at the beginning of the response curve due to the time delay present is reduced by 2.3% when compared to that of the delay-based ADRC structure. Further, at 40 s when step output disturbance is applied (refer to Figure 9a–e), the amplitude of the output disturbance undershoot is reduced by around 25% to 27% in the proposed design, as compared to that of the time-delay-based ADRC structure.
4. A comparison of the rise times in Table 5 shows that the proposed and modified ADRC methods have similar small rise times ( $T_r$ ), in contrast to the high rise time for the ESPO method. This indicates that the proposed method shows acceptable behaviour by not making the system slower or unstable, unlike the ESPO design.
5. Hence, it can be noted from Figures 8 and 9 that the proposed predictive method for the Type 1 system showed more robustness by better compensating both system input and output disturbances with noise under existing time delay, as compared to the considered delay-based ADRC and ESPO methods.

#### 4.3. Experiment 3: Second-Order Type 2 System

The Type 2 system studied in this paper is given by its transfer function and state-space model presented in Equations (27) and (28).

$$G_{Type2}(s) = \frac{1}{s^2} e^{-\tau s}; \tau = 0.1s \quad (27)$$

$$\begin{cases} \dot{x} = Ax + Bu \\ y = Cx(t - \tau) \\ \text{where } A = \begin{bmatrix} 0 & 1 \\ 0 & 0 \end{bmatrix}, B = \begin{bmatrix} 0 \\ 1 \end{bmatrix}, C = [1 \ 0] \end{cases} \quad (28)$$

Figures 10 and 11 illustrate the responses for the Type 2 system, firstly for the case of only input disturbance ( $C_1, C_2, C_3, C_4, C_5$ ) applied and secondly for the case of both input disturbance and step output disturbance applied with time delay present. Results for the different evaluation indicators are reported in Tables 6 and 7.

The following observations are noted for the Type 2 system, using the performance index values seen in Tables 6 and 7:

1. The overshoot (OS) at the start of the response due to time delay is decreased by 9.1% for the proposed structure when compared to that of the modified ADRC (refer to Figures 10b and 11b). In addition, there is a decrease in the time width of the startup overshoot by 67.607% in the proposed design.
2. As shown in Table 7, the maximum drop from reference due to output disturbance ( $d_{m,o}$ ) is less for the proposed design when compared with that of the modified ADRC. Thus,  $d_{m,o}$  is greatly reduced by around 59% to 61% in the proposed design, as compared to that of the modified ADRC structure (refer to Figure 11a–e). However, the adjustment time needed to return to reference ( $T_a$ ) is similar for both the former and latter methods, whereas the response of the ESPO design becomes unstable when step output disturbance is applied at 40 s (refer to Table 7).

3. Table 6 shows that the ITAE values for the proposed design are comparatively smaller value than those of the modified ADRC. For example, for  $C_2$  input and step output disturbances present, the proposed system has ITAE values of 11.6360 (from 0 s to 40 s), 76.9720 (from 40 s to 80 s), and 88.5950 (from 0 s to 80 s), whereas the corresponding ITAE values for ADRC are relatively higher, and the ESPO shows unstable behaviour due to the step output disturbance applied.
4. A comparison of the rise time ( $T_r$ ) values in Table 7 shows that the modified ADRC and proposed methods have approximately similar readings, unlike the slightly higher rise times such as 2.110 s seen for the ESPO design.
5. Therefore, Figures 10 and 11 show that the novel proposed design for the Type 2 system proved more robust when dealing with external disturbances and noise under time delay, compared to the modified delay-based ADRC and ESPO methods.

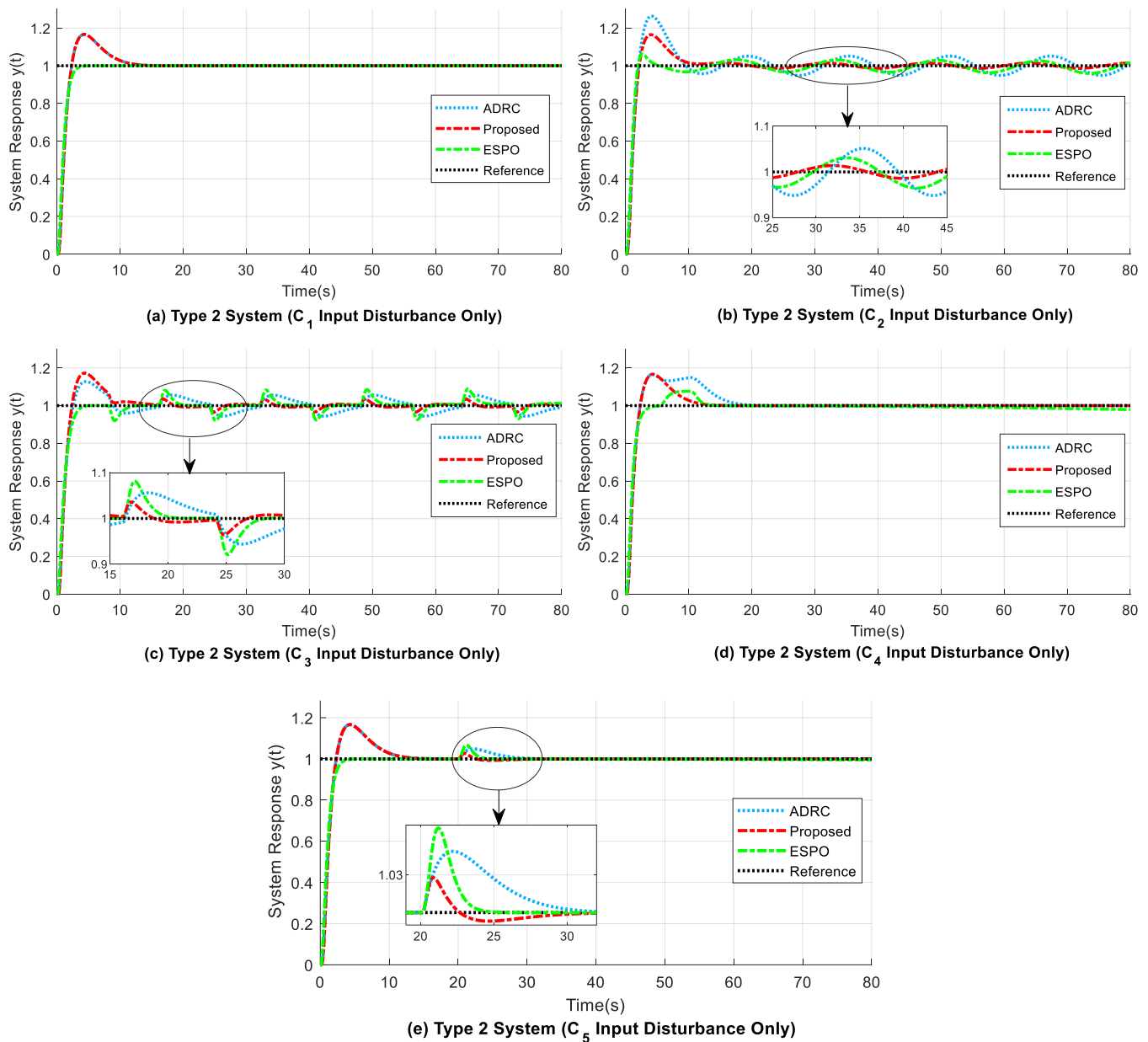


**Figure 10.** Responses for the case of only input disturbances are presented for the Type 2 system: (a) only  $C_1$  input disturbance present; (b) only  $C_2$  input disturbance present; (c) only  $C_3$  input disturbance present; (d) only  $C_4$  input disturbance present; (e) only  $C_5$  input disturbance present.

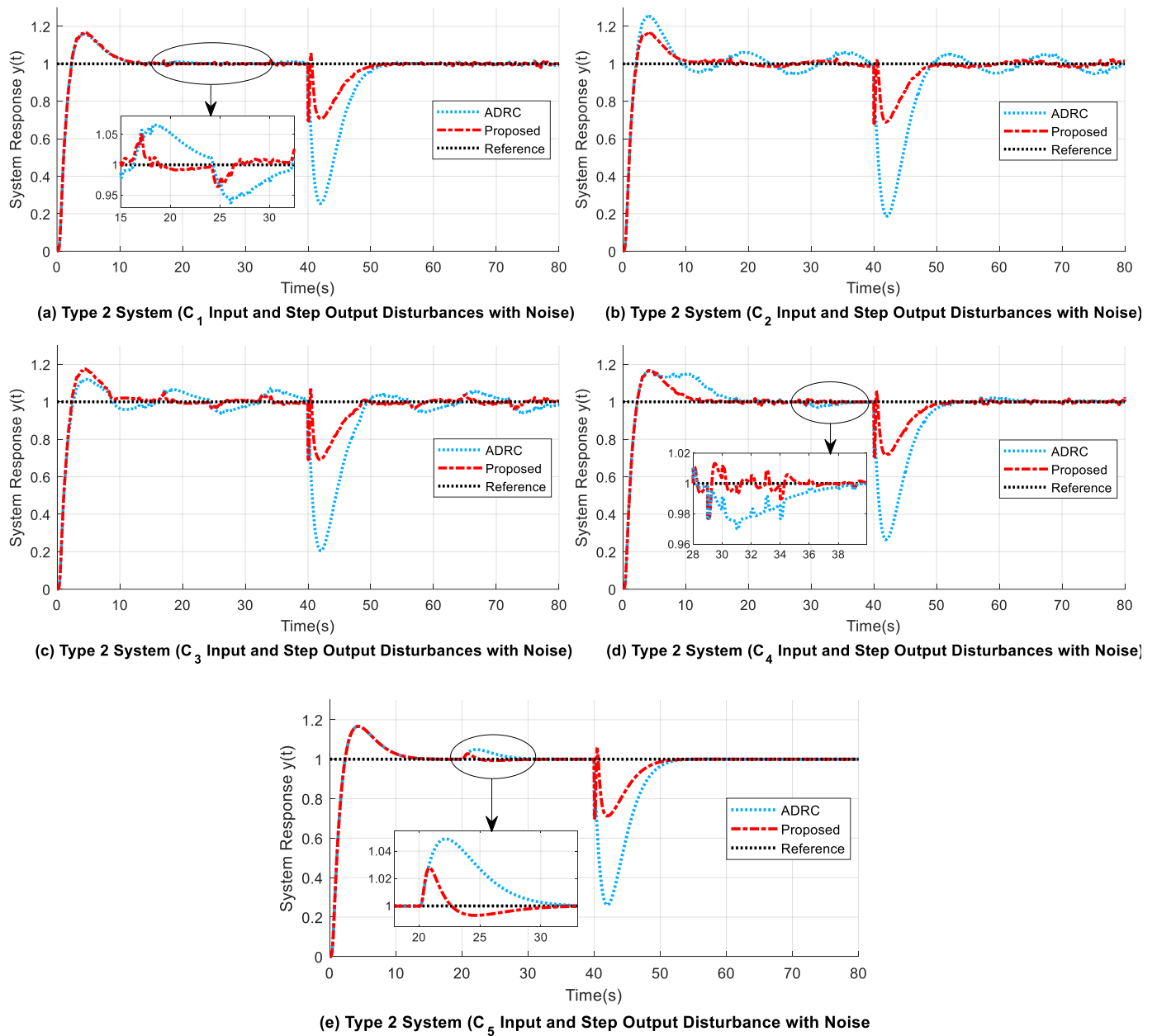


**Figure 11.** Responses for the different input disturbances and step output disturbance with noise for the Type 2 system: (a)  $C_1$  of  $\delta_1(x(t), t)$ ,  $\delta_2(x(t), t)$ , and noise present; (b)  $C_2$  of  $\delta_1(x(t), t)$ ,  $\delta_2(x(t), t)$ , and noise present; (c)  $C_3$  of  $\delta_1(x(t), t)$ ,  $\delta_2(x(t), t)$ , and noise present; (d)  $C_4$  of  $\delta_1(x(t), t)$ ,  $\delta_2(x(t), t)$ , and noise present; (e)  $C_5$  of  $\delta_1(x(t), t)$ ,  $\delta_2(x(t), t)$ , and noise present.

**Table 6.** ITAE performance index values for Type 2 system.

Input Disturbance Number	Method	With Input Disturbance ( $C_i$ ) *			With Input Disturbance ( $C_i$ ) *, Output Disturbance, and Noise		
		ITAE (0–40 s)	ITAE (40–80 s)	ITAE (0–80 s)	ITAE (0–40 s)	ITAE (40–80 s)	ITAE (0–80 s)
$i = 1$	ADRC	5.6431	$1.3318 \times 10^{-6}$	5.6431	8.3739	167.5400	175.9000
	Proposed	5.6431	$1.3318 \times 10^{-6}$	5.6431	<b>7.4086</b>	<b>68.3370</b>	<b>75.7330</b>
	ESPO	<b>0.8550</b>	<b><math>5.0639 \times 10^{-12}</math></b>	<b>0.8550</b>	Unstable	Unstable	Unstable
$i = 2$	ADRC	29.9070	77.8620	107.7700	32.2100	229.5100	261.7100
	Proposed	<b>11.3450</b>	<b>21.2620</b>	<b>32.6060</b>	<b>11.6360</b>	<b>76.9720</b>	<b>88.5950</b>
	ESPO	16.5060	51.3300	67.8250	Unstable	Unstable	Unstable
$i = 3$	ADRC	27.8760	78.8290	106.7000	30.1880	230.4000	260.5800
	Proposed	<b>12.4240</b>	<b>23.7290</b>	<b>36.1520</b>	<b>12.6680</b>	<b>79.5770</b>	<b>92.2330</b>
	ESPO	13.9060	48.5680	62.4720	Unstable	Unstable	Unstable
$i = 4$	ADRC	14.5970	$5.9430 \times 10^{-6}$	14.5970	19.7420	168.6300	188.3600
	Proposed	<b>5.6431</b>	<b><math>1.3318 \times 10^{-6}</math></b>	<b>5.6431</b>	<b>8.0527</b>	<b>65.4530</b>	<b>73.4940</b>
	ESPO	5.6828	29.7870	35.4680	Unstable	Unstable	Unstable
$i = 5$	ADRC	11.3930	0.0021	11.3950	13.9520	167.5400	181.4800
	Proposed	7.2863	<b>0.0007</b>	<b>7.2871</b>	<b>8.6107</b>	<b>68.3360</b>	<b>76.9340</b>
	ESPO	<b>3.4259</b>	5.3366	8.7624	Unstable	Unstable	Unstable

\*  $C_i$  is input disturbance that corresponds to input disturbance number  $i$  ( $C_1, C_2, C_3, C_4, C_5$  of  $\delta_1(x(t), t)$ ).

**Table 7.** Other performance index values for Type 2 system.

Input Disturbance Number	Method	With Input Disturbance ( $C_i$ ) *			With Input Disturbance ( $C_i$ ) *, Output Disturbance, and Noise			
		OS (%)	$T_r$ (s)	$D_{m,i}$	OS (%)	$T_r$ (s)	$d_{m,o}$	$T_a$ (s)
$i = 1$	ADRC	16.6700	1.4293	$\approx 0$	<b>15.8700</b>	<b>1.4109</b>	0.7458	13.5400
	Proposed	16.6700	<b>1.4293</b>	$\approx 0$	16.9300	1.4319	<b>0.3056</b>	<b>13.3700</b>
	ESPO	$\approx 0$	1.6790	$\approx 0$	Unstable	Unstable	Unstable	Unstable
$i = 2$	ADRC	26.3700	1.2905	0.0510	25.3900	<b>1.2759</b>	0.8127	<b>9.3700</b>
	Proposed	<b>16.5000</b>	1.3158	0.0310	<b>16.2900</b>	1.3255	<b>0.3199</b>	10.4100
	ESPO	6.1900	<b>1.2815</b>	<b>0.0140</b>	Unstable	Unstable	Unstable	Unstable
$i = 3$	ADRC	12.7700	1.5407	0.0560	<b>12.0000</b>	1.5804	0.7948	9.4900
	Proposed	17.2700	<b>1.4737</b>	<b>0.0360</b>	17.6000	<b>1.5254</b>	<b>0.3090</b>	<b>8.5700</b>
	ESPO	<b>0.0400</b>	2.1103	0.0820	Unstable	Unstable	Unstable	Unstable
$i = 4$	ADRC	16.5000	<b>1.4045</b>	0.1670	<b>16.5900</b>	<b>1.4482</b>	0.7361	15.9500
	Proposed	16.6700	1.4293	<b>0.1670</b>	16.7600	1.4963	<b>0.2961</b>	<b>15.9500</b>
	ESPO	<b>7.6300</b>	1.5489	0.0760	Unstable	Unstable	Unstable	Unstable
$i = 5$	ADRC	16.6700	1.4293	0.0490	<b>15.8700</b>	<b>1.4109</b>	0.7459	13.5500
	Proposed	16.6700	<b>1.4293</b>	<b>0.0300</b>	16.9300	1.4319	<b>0.3057</b>	<b>13.3700</b>
	ESPO	<b>6.7600</b>	1.6559	0.0680	Unstable	Unstable	Unstable	Unstable

\*  $C_i$  is input disturbance that corresponds to input disturbance number  $i$  ( $C_1, C_2, C_3, C_4, C_5$  of  $\delta_1(x(t), t)$ ).

4.4. Effect of Control Signal  $u$  and ESO States ( $z_2$  and  $z_3$ )

Figure 12a,b show that the control variable  $u$  is plotted for an ESPO design for a Type 0 system, containing both step input and step output disturbances with and without noise, respectively. It is visible from this figure that the control signal does contain a non-zero steady state, which means the control cost or energy needed to maintain the control

performance is high. The control signals for Type 1 and 2 systems have not been indicated here because they are unstable when controlled by the ESPO-based controller, with step output disturbance and white noise present in the system.

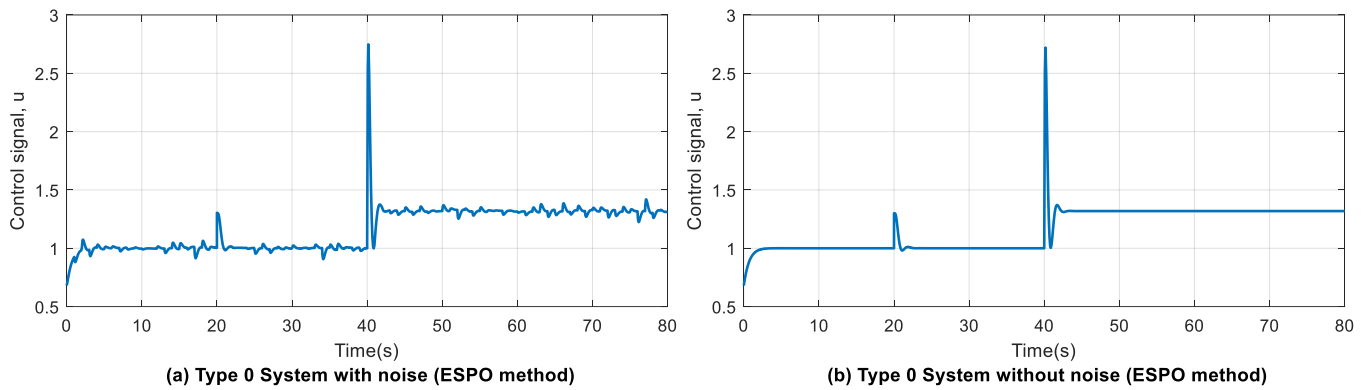


**Figure 12.** Control signal  $u$  for Type 0 system with step input disturbance and step output disturbance using ESPO method: (a) with measurement noise; (b) without measurement noise.

The plots of the control variable  $u$  for the considered ADRC and proposed methods are presented in Figure 13. It is known that measurement noise adversely affects the output time response by introducing significant oscillations in the output response curve. Thus, from Figure 13d–f, it can be interpreted that the proposed method has a negligible effect of noise on the control variable  $u$ .

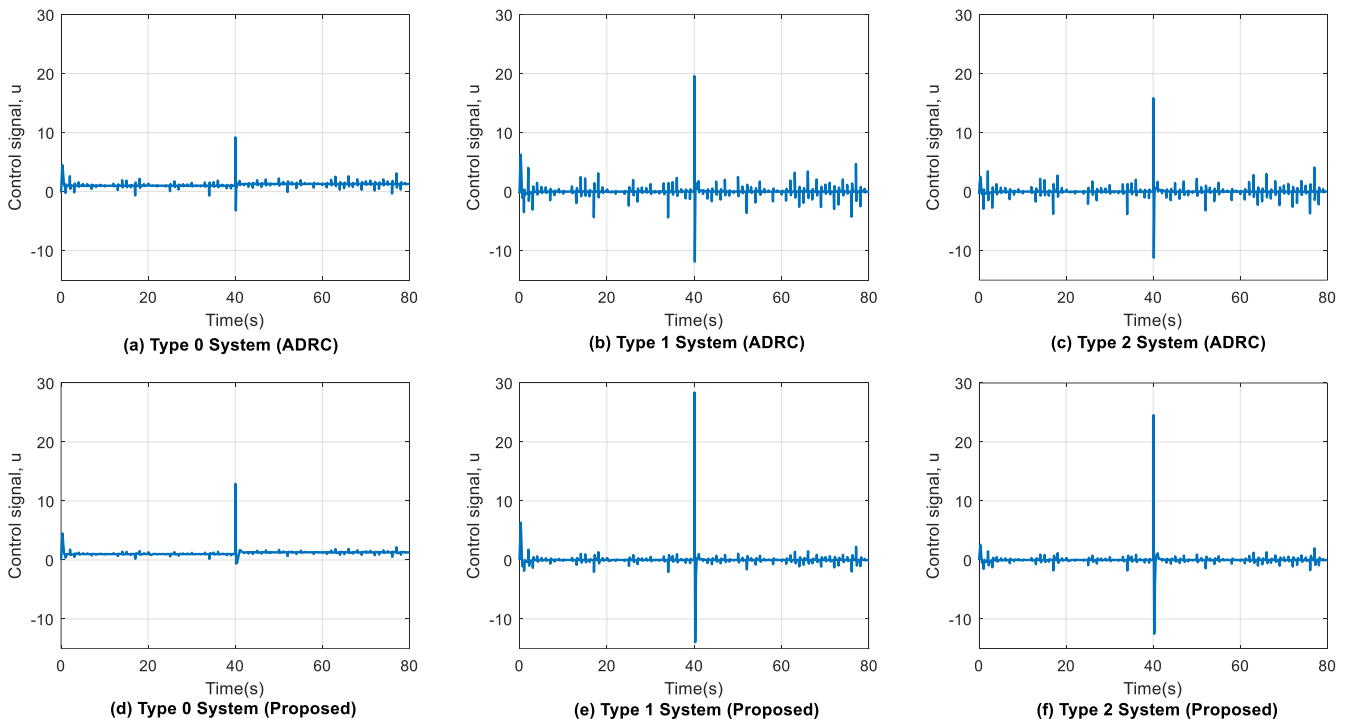


**Figure 13.** Control signal  $u$  with step input disturbance, step output disturbance, and measurement noise for all types of systems: (a–c) modified time-delay-based ADRC method; (d–f) proposed method.

Furthermore, Figures 14 and 15 indicate the estimated states  $z_2$  and  $z_3$ , respectively, of the time-delay-based ADRC and the proposed controller. These states are generated from the ESO component of the ADRC. Figures 14a–c and 15a–c show that the estimated states of the modified delay-based ADRC structure are affected by the white noise signal present at the system output. This is contrary to the case of the proposed controller, as seen in Figures 14d–f and 15d–f, wherein the measurement noise had a negligible effect

on the estimated states  $z_2$  and  $z_3$ . Furthermore, in the case of the step output disturbance being applied at 40 s, the zoomed plots of Figure 14 indicate a speedy disturbance recovery in the proposed design, illustrating its advantage over the associated ADRC model.

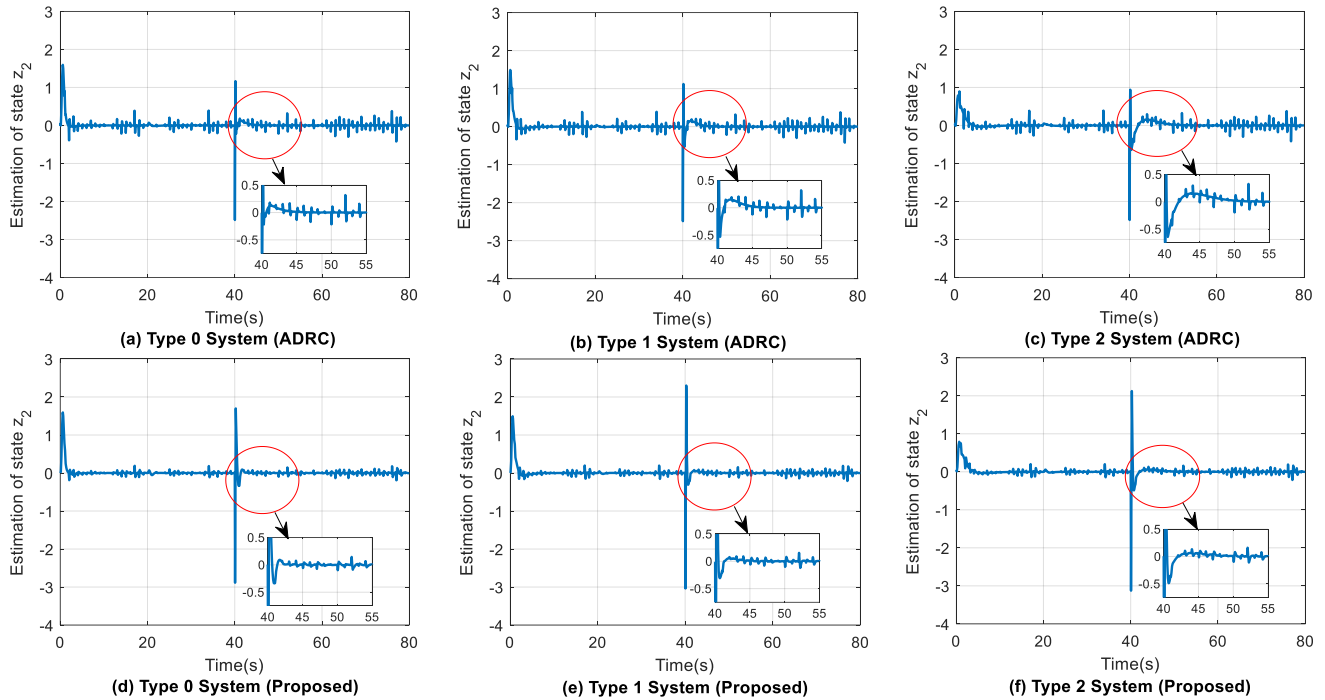


**Figure 14.** Estimated state  $z_2$  with step input disturbance, step output disturbance, and measurement noise for all types of systems: (a–c) modified time-delay-based ADRC method; (d–f) proposed method.

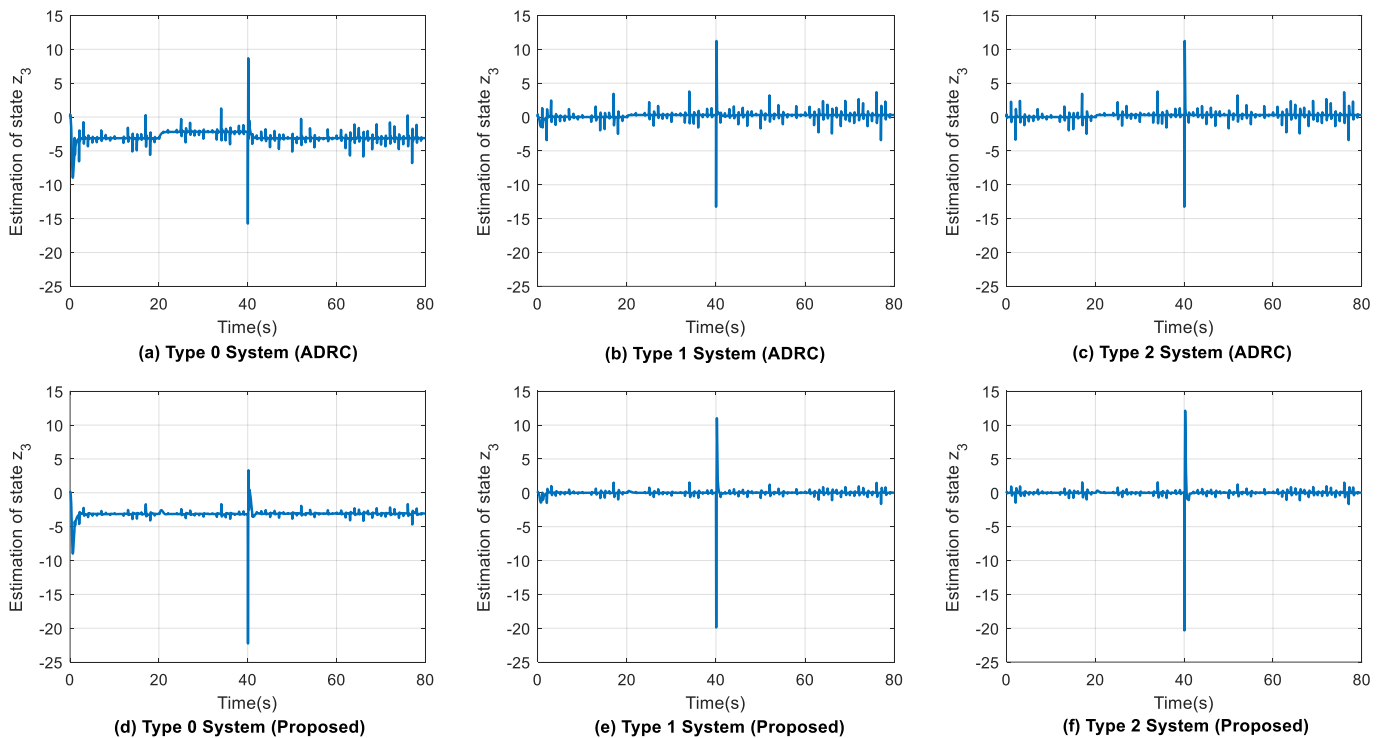


**Figure 15.** Estimated state  $z_3$  with step input disturbance, step output disturbance, and measurement noise present for all types of systems: (a–c) modified time-delay-based ADRC method; (d–f) proposed method.

#### 4.5. Effect of Change in Time Delay

This subsection presents the results of testing the effect of change in time delay ( $\tau$ ). In this experiment, the periodic form of input disturbance ( $C_2$ ) and step output disturbance were applied. In Figure 16 (Type 0 system), Figure 17 (Type 1 system), and Figure 18 (Type 2 system), the delay design ( $\tau_d$ ) for the ADRC and ESPO and the system delay ( $\tau_s$ ) are the same. This is simulated to assess the case in which the system delay is known. In this case, the design time-delay is tuned to the known system time-delay for time-delay compensation. Due to the smaller value of time delay (0.1 s), in Figures 16a, 17a, and 18a, the oscillations appear to be of smaller amplitude as compared to the responses shown in Figures 16b, 17b, and 18b that correspond to cases of higher time-delays (1 s for Type 0 system, 0.3 s for both Type 1 and Type 2 systems). Therefore, it is visible that the proposed design performed better than the other two methods for a higher time-delay (greater than 0.1 s) since its response curves are less oscillatory with quick output disturbance compensation. In Figures 17b and 18b, it is important to note that the plots of ESPO-based controllers are not present due to their unstable nature under the impact of output disturbance applied to the system. Moreover, the proposed design shows a positive spike at the start of the step output disturbance applied at 40 s, indicating rapid behaviour. However, this spike can be reduced by decreasing  $\omega_e$ . Furthermore, as seen from the zoomed plots in Figures 16–18, the adjustment time  $T_a$  to return to reference when step output disturbance is applied is smaller for the proposed design. Hence, the proposed design improved the system response by using a predictive mechanism (ESPO) that can compensate for these uncertainties as a disturbance.

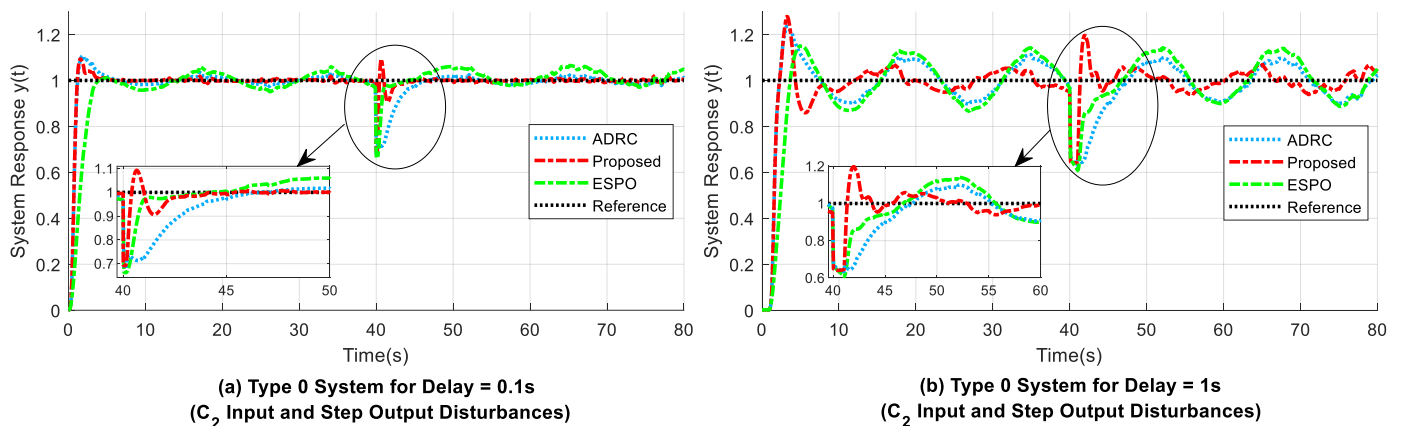


Figure 16. Test on changes in time delay ( $\tau_d = \tau_s = \tau$ ): (a) Type 0 system at  $\tau = 0.1$  s; (b) Type 0 system at  $\tau = 1$  s.

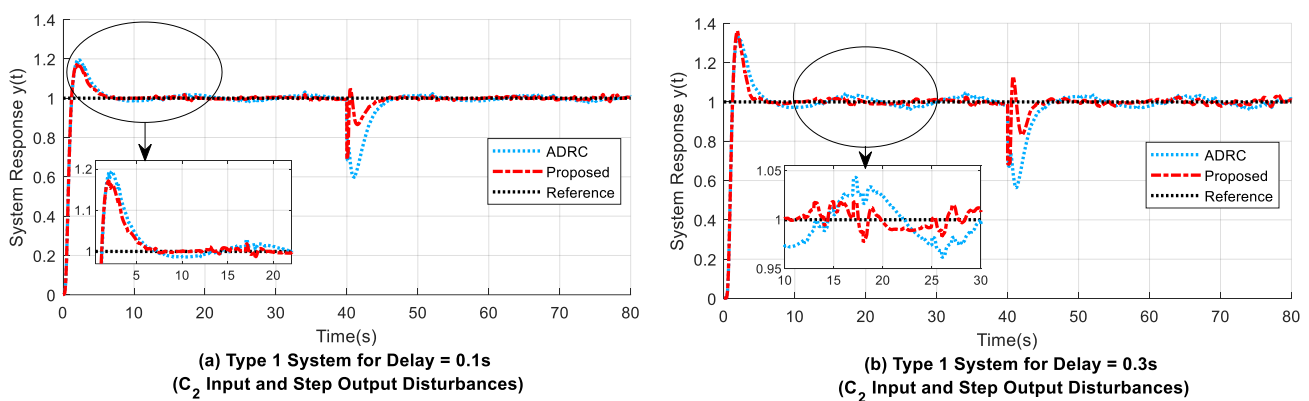
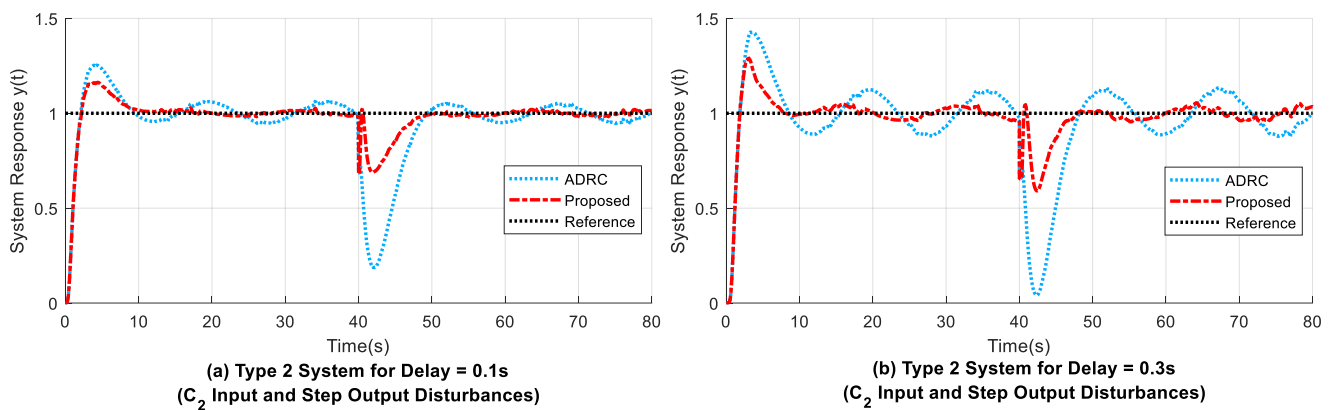


Figure 17. Test on changes in time delay ( $\tau_d = \tau_s = \tau$ ): (a) Type 1 system at  $\tau = 0.1$  s; (b) Type 1 system at  $\tau = 0.3$  s.



**Figure 18.** Test on changes in time delay ( $\tau_d = \tau_s = \tau$ ): (a) Type 2 system at  $\tau = 0.1$  s; (b) Type 2 system at  $\tau = 0.3$  s.

However, as seen in Figures 17b and 18b, second-order Type 1 and Type 2 systems present a more significant problem when examining the impact of change in time delay due to their frequently more aggressive dynamics than Type 0 systems. Hence, Type 1 and Type 2 systems were tested at a lower delay because, for values greater than 0.3 s, the observed overshoot at the beginning of the response curve was high.

In addition, for testing the robustness of the proposed controller method for different known values of system delay, the experiment for the robustness to both disturbances and time-varying time-delay (TVTD) of the system ( $\tau_s$ ) was conducted for the different second-order system types, as seen in Figure 19. The input disturbance ( $C_2$ ) and step output disturbance were applied. In Figure 19, the delay designed for the ADRC and ESPO ( $\tau_d$ ) and the system delay ( $\tau_s$ ) are different. This is simulated for the case of a system containing unexpected delay values that are unknown to the operator or the designer. Three examples of unexpected system delays are shown in Figure 19: a case where the time-varying time-delay of the system varies between 0 s and 0.4 s when the design delay for the ADRC and ESPO is 0.1 s, a case where the system delay is 0.2 s when the design delay for the ADRC and ESPO is 0.1 s, and a case where the design delay of ESPO and ADRC is greater than 0.1 s. For the last case, the Type 0 system is evaluated for a time-varying time-delay of the system that varies from 0.9 to 1.3 s when the design delay of ADRC and ESPO is 1 s. However, for the evaluation of the design delay greater than 0.1 s, the Type 1 and Type 2 systems are assessed for time-varying time-delay of the system that varies from 0.2 to 0.5 s when the design delay is just 0.3 s owing to the complex dynamics of the two systems. It is observed that the compensation of the disturbances is achieved when the system delay deviates from the design delay. The system's stability is also maintained, but the response is generally affected, especially during the transient periods. Extensive research on time-delay compensation for the proposed controller method is necessary in future studies.

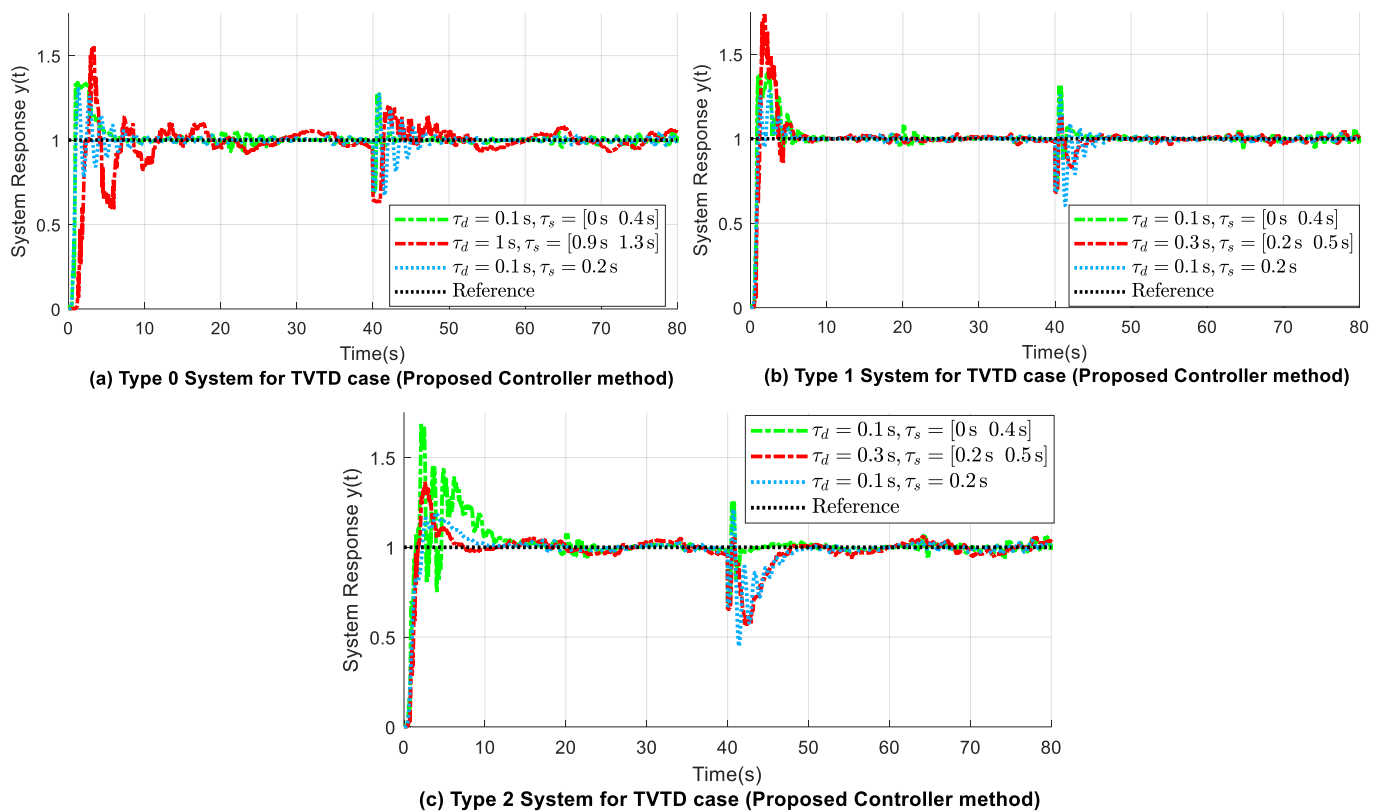


**Figure 19.** Test on time-varying time-delay (TVTD) case of the proposed controller design with  $\tau_d$  as the design delay and  $\tau_s$  as the system delay: (a) Type 0 system; (b) Type 1 system; (c) Type 2 system.

## 5. Discussion

This paper introduced a consolidated design incorporating the advantages of ADRC with the ESPO controller design. This section discusses and highlights the proposed controller design's predictive characteristic that can enhance the disturbance and measurement noise compensation under time-delay control. The benefit of the presented design is related to satisfactory stability attained, improved transient response in the presence of time delay, and reasonable control of output disturbance compensation and noise, as observed from the responses presented in Section 4.

### 5.1. Disturbance Compensation with Noise and Time Delay

There are two properties when dealing with the time-delay problem. Firstly, time delays cause signals to arrive later. Secondly, time delays cause systems to become more oscillatory and unstable. However, as seen in Figures 6–11, the proposed controller had conquered these vibrations to a certain extent as opposed to the time-delay-based ADRC and ESPO methods.

Figures 6, 8, and 10 showed that the modified time-delay-based ADRC model did compensate for the input disturbance using its mechanism without the need for the ESPO. However, for the same cases, when step output disturbance was applied, it was noted that the novel proposed controller performed much better by attaining both quick output disturbance and noise compensation with time delay (refer to Figures 7, 9, and 11). This is because the internal dynamics that were modelled during the time-delay with the noise present were estimated, compensated, and removed significantly using the predictive idea. This compensation was inferred from the removal of the estimated disturbance  $\hat{\delta}(t)$  present in the proposed control law  $u_P(t)$  given by Equation (19).

### 5.2. Rise Time and Bandwidth

The ESPO structure's input signal  $r(t) = [1 \ 0]^T$  is analogous to the tracking (reference step signal) and differentiated signals generated by the TD in both the modified ADRC and proposed predictive methods. In the Type 2 system, for the case of only input disturbance present, the ESPO response is more steered than the proposed design due to the overly gentle TD inside the proposed design. Hence, the rise in the signal seen in Figure 10 for the proposed method is slow compared to that of the ESPO method. Due to the ESPO's dependence on specific  $K$  values, it has the advantage of having less overshoot than the time-delay-based ADRC and proposed controller methods. However, the ESPO shows an unsteady performance when step output disturbance is applied for both Type 1 and Type 2 systems (refer to Figures 9 and 11).

Furthermore, observer bandwidth  $\omega_e$  affects the ESPO in two ways: the shift in the response curve and the oscillation amplitude. Thus, the proposed method containing the ESPO-based controller is dependent on  $\omega_e$  as well. However, an improved response for the proposed design can be obtained by further tuning the ESPO bandwidth.

### 5.3. Stability Analysis

One commonly used method to analyze the stability of control systems is the frequency response method using an open-loop Bode diagram. The Bode diagram constitutes two graphs, the magnitude plot indicating the gain margin (Gm) in decibels and the phase plot indicating the phase margin (Pm) in degrees. This section presents the stability analysis of the novel controller proposed in this paper conducted using open-loop Bode diagrams. The Bode diagrams illustrating the frequency response of the linearized systems composed of the controlled objects and the proposed controller are provided in Figure 20, where the controlled object is a Type 0, Type 1, or Type 2 system.

In Figure 20a, for control of the Type 0 system (given in Equations (23) and (24)), the gain margin is 33.6 dB and the phase margin is  $143^\circ$  (deg). The delay margin obtained was at 1.41 s; for extra time-delays less than 1.41 s, the Type 0 system is stable. Given that the Gm and Pm are positive, as seen in Figure 20a, the system is closed-loop stable. The stability is further validated by seeing that the phase crossover frequency (7.61 Hz) is greater than the gain crossover frequency (0.281 Hz).

Figure 20b displays the stability margins for the Type 1 system (from Equations (25) and (26)) controlled by the proposed design. As seen in the open-loop Bode plots, the gain margin (Gm) is 29.6 dB at a phase crossover frequency of 5.42 Hz, whereas the phase margin is  $94.7^\circ$  at a gain crossover frequency of 0.338 Hz. Thus, the system analyzed is closed-loop stable. Moreover, as shown in the phase plot in Figure 20b, the delay margin obtained is 0.779 s. Hence, the system will be on the verge of instability when the system incurs an extra time-delay equal to the delay margin.

The open-loop Bode plots in Figure 20c provide the stability margins of the proposed control system for the Type 2 system given in Equations (27) and (28). The gain margin of the open-loop Bode plot is positive and decently large at 37.4 dB, with a phase gain margin of  $70.3^\circ$ . Thus, the system is closed-loop stable and will fall in instability outside stability margins (Gm and Pm). Further, the gain margin and phase margin occur at 5.26 Hz and 0.148 Hz crossover frequencies, respectively. In addition, from the phase plot, it was observed that the second-order Type 2 system analyzed is closed-loop stable for delay margins of less than 1.32 s.

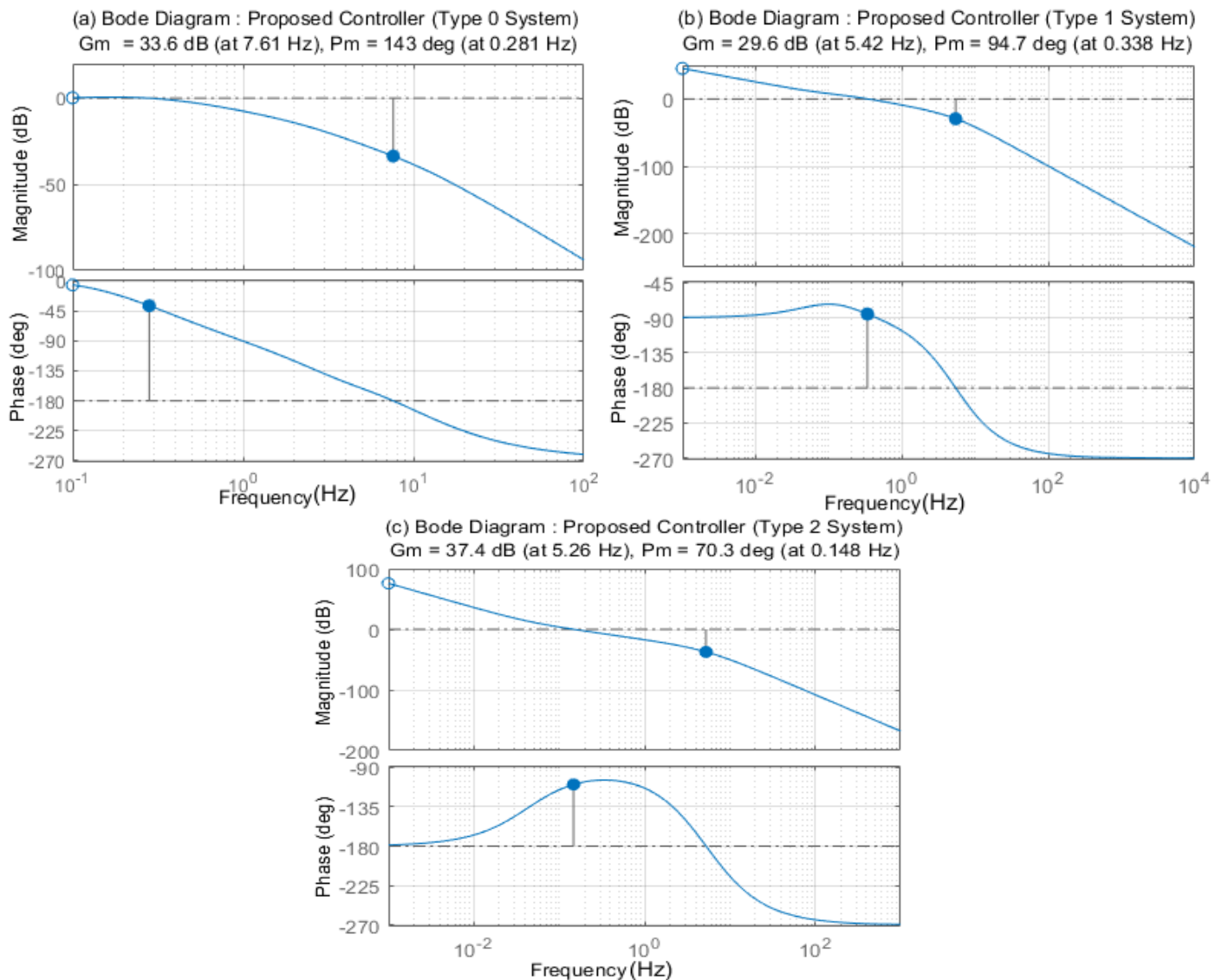


**Figure 20.** Bode plots showing stability margins using the proposed controller: (a) Type 0 system; (b) Type 1 system; (c) Type 2 system.

#### 5.4. Performance Criteria Analysis

For certain cases, the overshoot (OS) at the beginning of the response curve was reduced (refer to Figures 6–11), except for one case for the Type 2 system where  $C_3$  input disturbance is applied. From Table 3 and Figure 7b,c, for the case of the ESPO method (Type 0 system), it was seen that the response curve has an adjustment time ( $T_a$ ) of reaching reference signal at 4.24 s and 3.23 s, respectively. However, the system response is oscillatory after the step output disturbance is applied, and it is seen that the response curve gives a non-zero SSE, thus proving less robust behaviour in response to external (output) disturbance application. Furthermore, in the case of ESPO-based control for both Type 1 and Type 2 systems, when step output disturbance is applied, the ESPO is not steady. Thus, ESPO response curves were not plotted in Figures 9 and 11.

The proposed method showed a smaller adjustment time ( $T_a$ ) for disturbance recovery than the related ADRC and ESPO methods individually (in Figures 7, 9, and 11). This observation is further substantiated by comparing the maximum deviation ( $D_{m,i}$ ) and drop ( $d_{m,o}$ ) in the response curve at instants when both input and output disturbances are applied. For the proposed design, the absolute value of this drop and the deviation from the reference signal are the least in most cases compared to the other methods. Thus, the

proposed method showed more stable action and is faster in returning to the zero SSE (refer to Figures 9 and 11). However, the proposed method experiences a jump due to a shorter recovery time after applied output disturbance. This is visible in Figures 7, 9, and 11. This jump can be further reduced by tuning the proposed controller parameters.

Experiments show that the time-delay-based ADRC and the proposed structures had approximately similar rise times ( $T_r$ ). However, the proposed method showed a smaller  $T_r$  in most cases for all system types (refer to Tables 3, 5, and 7) compared to the ESPO method. Thus, having a reasonable rise time adds to the proposed structure's characteristics by not making the entire system unstable or slowly approaching the steady state.

## 6. Conclusions and Future Recommendations

This paper proposed a novel controller design in which the hybridization of delay-based ADRC and ESPO-based controller methods has combined their benefits. The former relies on minimal model information containing the ESO to timely estimate and compensate for the disturbance using NLSEF. The latter method uses an extended state for the conventional PO due to its robust behaviour when estimating and cancelling total disturbances with sensor delay. The experimental analysis and performance criteria noted from the simulation results presented in this study support the application of the proposed "predictive ESO-based ADRC" controller design in time-delay control applications involving different external disturbances.

When performing the disturbance compensation, the novel predictive controller proposed in this paper conquered the internal dynamics generated during the existing time delay by considering the internal dynamics as a disturbance. In addition, the oscillations arising due to the time delay present in the total system were suppressed to an acceptable degree by this novel predictive approach. Thus, when both internal and external disturbances are introduced, the proposed controller enjoys a stable tracking response and shows decent reliability and robust behaviour. Additionally, the system shows a reasonable level of noise reduction. Therefore, these findings channel future research by tapping into a new dimension of controller design.

Future research should improve the proposed predictive ESO-based ADRC algorithm by further reducing the initial overshoot seen in the transient response curve, along with the spike obtained at the start of the external step output disturbance. This improvement will involve further tuning the proposed controller parameters, such as the NLSEF parameters and the observer bandwidth ( $\omega_e$ ). Further, control of higher-order systems ( $n$ -dimensional states) by the proposed controller, robustness analysis for the case of system parameter perturbations, assessment of bigger time delay, and comprehensive research on time-delay compensation will form part of future work. Application-wise, control of the developed human-machine interface platform (seen in [49]) by the proposed algorithm of this paper, along with its stability and transparency analysis, can serve in the future as a worthwhile contribution to the field of control systems theory and bilateral teleoperation applications.

**Author Contributions:** Conceptualization, S.D. and S.N.F.N.; methodology, S.N.F.N. and S.D.; software, S.N.F.N. and S.D.; validation, S.N.F.N., S.D. and B.J.v.W.; formal analysis, S.N.F.N. and S.D.; writing—original draft preparation, S.N.F.N.; writing—review and editing, S.D., S.N.F.N. and B.J.v.W.; supervision—S.D. and B.J.v.W. All authors have read and agreed to the published version of the manuscript.

**Funding:** This work is based on the research supported in part by the National Research Foundation of South Africa (Grant Numbers 98398 and 138783).

**Institutional Review Board Statement:** Not applicable.

**Informed Consent Statement:** Not applicable.

**Data Availability Statement:** Not applicable.

**Conflicts of Interest:** The authors declare no conflict of interest.

## References

1. Hokayem, P.F.; Spong, M.W. Bilateral teleoperation: An historical survey. *Automatica* **2006**, *42*, 2035–2057. [[CrossRef](#)]
2. Richard, J.-P. Time-delay systems: An overview of some recent advances and open problems. *Automatica* **2003**, *39*, 1667–1694. [[CrossRef](#)]
3. Shahbazi, M.; Atashzar, S.F.; Patel, R. A Systematic Review of Multilateral Teleoperation Systems. *IEEE Trans. Haptics* **2018**, *11*, 338–356. [[CrossRef](#)] [[PubMed](#)]
4. Nahri, S.N.F.; Du, S.; Van Wyk, B.J. A Review on Haptic Bilateral Teleoperation Systems. *J. Intell. Robot. Syst.* **2022**, *104*, 13. [[CrossRef](#)]
5. Han, J. A class of extended state observers for uncertain systems. *Control Decis.* **1995**, *10*, 85–88.
6. Han, J.Q. Auto Disturbance Rejection Controller and It's Applications. *Control Decis.* **1998**, *13*, 19–23. [[CrossRef](#)]
7. Han, J. From PID to Active Disturbance Rejection Control. *IEEE Trans. Ind. Electron.* **2009**, *56*, 900–906. [[CrossRef](#)]
8. Gao, Z. On the centrality of disturbance rejection in automatic control. *ISA Trans.* **2014**, *53*, 850–857. [[CrossRef](#)]
9. Feng, H.; Guo, B.-Z. Active disturbance rejection control: Old and new results. *Annu. Rev. Control* **2017**, *44*, 238–248. [[CrossRef](#)]
10. Chu, Z.; Wu, C.; Sepeshri, N. Active disturbance rejection control applied to high-order systems with parametric uncertainties. *Int. J. Control Autom. Syst.* **2019**, *17*, 1483–1493. [[CrossRef](#)]
11. He, T.; Wu, Z.; Li, D.; Wang, J. A tuning method of active disturbance rejection control for a class of high-order processes. *IEEE Trans. Ind. Electron.* **2019**, *67*, 3191–3201. [[CrossRef](#)]
12. Wu, Z.; Shi, G.; Li, D.; Liu, Y.; Chen, Y. Active disturbance rejection control design for high-order integral systems. *ISA Trans.* **2022**, *125*, 560–570. [[CrossRef](#)]
13. Wu, Z.; Gao, Z.; Li, D.; Chen, Y.; Liu, Y. On transitioning from PID to ADRC in thermal power plants. *Control Theory Technol.* **2021**, *19*, 3–18. [[CrossRef](#)]
14. Fareh, R.; Khadraoui, S.; Abdallah, M.Y.; Baziyad, M.; Bettayeb, M. Active disturbance rejection control for robotic systems: A review. *Mechatronics* **2021**, *80*, 102671. [[CrossRef](#)]
15. Nahri, S.N.F.; Du, S.; van Wyk, B.J. Active Disturbance Rejection Control Design for a Haptic Machine Interface Platform. *Adv. Sci. Technol. Eng. Syst. J.* **2021**, *6*, 898–911. [[CrossRef](#)]
16. Wang, F.; Liu, P.; Xie, M.; Jing, F.; Liu, B.; Cao, Y.; Ma, C. Robust Reduced-Order Active Disturbance Rejection Control Method: A Case Study on Speed Control of a One-Dimensional Gimbal. *Machines* **2022**, *10*, 592. [[CrossRef](#)]
17. Sun, A.; Songmao, P.; He, Z.; Xiao, K.; Sun, P.; Wang, P.; Wei, X. Application of model free active disturbance rejection controller in nuclear reactor power control. *Prog. Nucl. Energy* **2021**, *140*, 103907. [[CrossRef](#)]
18. Niculescu, S.-I. *Delay Effects on Stability: A Robust Control Approach*; Springer Science & Business Media: Berlin/Heidelberg, Germany, 2001; Volume 269.
19. Wang, L.; Li, Q.; Tong, C.; Yin, Y. Overview of active disturbance rejection control for systems with time-delay. *Control Theory Appl.* **2013**, *30*, 1521–1533. [[CrossRef](#)]
20. Chen, S.; Xue, W.; Zhong, S.; Huang, Y. On comparison of modified ADRCs for nonlinear uncertain systems with time delay. *Sci. China Inf. Sci.* **2018**, *61*, 70223. [[CrossRef](#)]
21. Xia, Y.; Liu, G.P.; Shi, P.; Han, J.; Rees, D. Active disturbance rejection control for uncertain multivariable systems with time-delay. *IET Control Theory Appl.* **2007**, *1*, 75–81. [[CrossRef](#)]
22. Pawar, S.N.; Chile, R.H.; Patre, B.M. Predictive extended state observer-based robust control for uncertain linear systems with experimental validation. *Trans. Inst. Meas. Control* **2021**, *43*, 2615–2627. [[CrossRef](#)]
23. Chen, G.; Liu, D.; Mu, Y.; Xu, J.; Cheng, Y. A Novel Smith Predictive Linear Active Disturbance Rejection Control Strategy for the First-Order Time-Delay Inertial System. *Math. Probl. Eng.* **2021**, *2021*, 5560123. [[CrossRef](#)]
24. Li, P.; Wang, L.; Zhu, G.; Zhang, M. Predictive active disturbance rejection control for servo systems with communication delays via sliding mode approach. *IEEE Trans. Ind. Electron.* **2020**, *68*, 12679–12688. [[CrossRef](#)]
25. Artheec Kumar, V.; Cao, Z.; Man, Z.; Chuei, R.; Bombuwela, D. Predictive extended state observer-based repetitive controller for uncertain systems with input delay. *Automatika* **2022**, *63*, 122–131. [[CrossRef](#)]
26. Wang, C.; Zuo, Z.; Qi, Z.; Ding, Z. Predictor-based extended-state-observer design for consensus of MASs with delays and disturbances. *IEEE Trans. Cybern.* **2018**, *49*, 1259–1269. [[CrossRef](#)] [[PubMed](#)]
27. Castillo, A.; Santos, T.L.; Garcia, P.; Normey-Rico, J.E. Predictive ESO-based control with guaranteed stability for uncertain MIMO constrained systems. *ISA Trans.* **2021**, *112*, 161–167. [[CrossRef](#)] [[PubMed](#)]
28. Zheng, Q.; Gao, Z. Predictive active disturbance rejection control for processes with time delay. *ISA Trans.* **2014**, *53*, 873–881. [[CrossRef](#)] [[PubMed](#)]
29. Xue, W.; Liu, P.; Chen, S.; Huang, Y. On Extended State Predictor Observer Based Active Disturbance Rejection Control for Uncertain Systems with Sensor Delay. In Proceedings of the 2016 16th International Conference on Control, Automation and Systems (ICCAS), Gyeongju, Korea, 16–19 October 2016; pp. 1267–1271.
30. Tan, W.; Fu, C. Analysis of Active Disturbance Rejection Control for Processes with Time Delay. In Proceedings of the 2015 American Control Conference (ACC), Chicago, IL, USA, 1–3 July 2015; pp. 3962–3967.
31. Zhang, B.; Tan, W.; Li, J. Tuning of Smith predictor based generalized ADRC for time-delayed processes via IMC. *ISA Trans.* **2020**, *99*, 159–166. [[CrossRef](#)]

32. Cheng, Y.; Chen, Z.; Sun, M.; Sun, Q. Active disturbance rejection generalized predictive control for a high purity distillation column process with time delay. *Can. J. Chem. Eng.* **2019**, *97*, 2941–2951. [[CrossRef](#)]
33. Fu, C.; Tan, W. Linear active disturbance rejection control for processes with time delays: IMC interpretation. *IEEE Access* **2020**, *8*, 16606–16617. [[CrossRef](#)]
34. Chen, S.; Xue, W.; Huang, Y.; Liu, P. On Comparison between Smith Predictor and Predictor Observer Based Adrcs for Nonlinear Uncertain Systems with Output Delay. In Proceedings of the 2017 American Control Conference (ACC), Seattle, WA, USA, 24–26 May 2017; pp. 5083–5088.
35. Zhao, S.; Gao, Z. Modified active disturbance rejection control for time-delay systems. *ISA Trans.* **2014**, *53*, 882–888. [[CrossRef](#)]
36. Wang, S.; Sun, G.; Liu, S. Active disturbance rejection sliding mode control for time-delay systems. *J. Syst. Simul.* **2019**, *31*, 102.
37. Ran, M.; Wang, Q.; Dong, C.; Xie, L. Active disturbance rejection control for uncertain time-delay nonlinear systems. *Automatica* **2020**, *112*, 108692. [[CrossRef](#)]
38. Wang, X.; Zhou, Y.; Zhao, Z.; Wei, W.; Li, W. Time-delay system control based on an integration of active disturbance rejection and modified twice optimal control. *IEEE Access* **2019**, *7*, 130734–130744. [[CrossRef](#)]
39. Zheng, Q.; Gao, L.Q.; Gao, Z. On Validation of Extended State Observer Through Analysis and Experimentation. *J. Dyn. Syst. Meas. Control* **2012**, *134*, 024505. [[CrossRef](#)]
40. YV Wen-bin, Y.D. Modeling and Simulation of an Active Disturbance Rejection Controller Based on Matlab/Simulink. *Int. J. Res. Eng. Sci.* **2015**, *3*, 62–69.
41. Han, J.-q. Auto disturbances rejection control technique. *Front. Sci.* **2007**, *1*, 24–31.
42. Jiang, P.; Hao, J.-Y.; Zong, X.-P.; Wang, P.-G. Modeling and Simulation of Active-Disturbance-Rejection Controller with Simulink. In Proceedings of the 2010 International Conference on Machine Learning and Cybernetics, Qingdao, China, 11–14 July 2010; pp. 927–931.
43. Gao, Z. Scaling and Bandwidth-Parameterization Based Controller Tuning. In Proceedings of the American Control Conference, Denver, CO, USA, 4–6 June 2003; pp. 4989–4996.
44. Yoo, D.; Yau, S.-T.; Gao, Z. Optimal fast tracking observer bandwidth of the linear extended state observer. *Int. J. Control* **2007**, *80*, 102–111. [[CrossRef](#)]
45. Zhang, X.; Zhang, X.; Xue, W.; Xin, B. An overview on recent progress of extended state observers for uncertain systems: Methods, theory, and applications. *Adv. Control Appl. Eng. Ind. Syst.* **2021**, *3*, e89. [[CrossRef](#)]
46. Martins, F.G. Tuning PID controllers using the ITAE criterion. *Int. J. Eng. Educ.* **2005**, *21*, 867.
47. Saraswat, M.; Sharma, A. Genetic Algorithm for optimization using MATLAB. *Int. J. Adv. Res. Comput. Sci.* **2013**, *4*, 155–159.
48. Rasolomampionona, D.; Klos, M.; Cirit, C.; Montegiglio, P.; De Tuglie, E.E. A New Method for Optimization of Load Frequency Control Parameters in Multi-Area Power Systems Using Genetic Algorithms. In Proceedings of the 2022 IEEE International Conference on Environment and Electrical Engineering and 2022 IEEE Industrial and Commercial Power Systems Europe (EEEIC/I&CPS Europe), Prague, Czech Republic, 28 June–1 July 2022; pp. 1–9.
49. Nahri, S.N.F.; Du, S.; Van Wyk, B. Haptic System Interface Design and Modelling for Bilateral Teleoperation Systems. In Proceedings of the 2020 International SAUPEC/RobMech/PRASA Conference, Cape Town, South Africa, 29–31 January 2020; pp. 1–6.

**Disclaimer/Publisher’s Note:** The statements, opinions and data contained in all publications are solely those of the individual author(s) and contributor(s) and not of MDPI and/or the editor(s). MDPI and/or the editor(s) disclaim responsibility for any injury to people or property resulting from any ideas, methods, instructions or products referred to in the content.